NASA Technical Memorandum 100743

Radial Deformation of the Earth by Oceanic Tidal Loading

R. D. Ray and B. V. Sanchez

July 1989

NASA

NASA Technical Memorandum 100743

Radial Deformation of the Earth by Oceanic Tidal Loading

R. D. Ray
ST Systems Corporation
Lanham, Maryland

B. V. Sanchez
Goddard Space Flight Center
Greenbelt, Maryland

National Aeronautics and
Space Administration

Goddard Space Flight Center
Greenbelt, MD

1989

Abstract

A high-degree spherical harmonic series is used to compute the radial deformation of the Earth by oceanic tidal loading. By exploiting "fast" numerical transforms, this approach is found to be much more efficient—but no less accurate—than the traditional Green's function approach. The method is used to derive an atlas of load tide maps for 10 constituents of the NSWC ocean tide model.

1 Introduction

Tidal deformations of the Earth affect a wide range of geophysical and geodetic measurements (*Baker*, 1984; *Lambeck*, 1988). This is particularly true for the modern, high-precision techniques of space geodesy: satellite and lunar laser ranging, very long baseline interferometry, and satellite altimetry are all seriously affected by the deformation in their range measurements and/or their inferred baselines to other stations. Our purpose here is to discuss one particular type of deformation—radial deformation due to ocean loading—and to present an atlas of maps displaying this deformation for some of the major tidal constituents.

Our primary motivation in producing such an atlas is to provide an additional correction to satellite altimeter measurements. The range of the loading tide can easily reach 10 cm, and this is far too large an error source to ignore—compare, for example, the stringent requirements of the TOPEX error budget as listed by *Born et al.* (1984).

In satellite altimetry, only the geocentric tide ζ_g can be directly observed. This tide consists of a body tide ζ_b, a land-relative ocean tide ζ_o, and a load tide ζ_l:

$$\zeta_g = \zeta_b + \zeta_o + \zeta_l.$$

The body tide is relatively well understood and requires for its accurate evaluation only the astronomical, tidal-generating potential (given by *Cartwright & Edden* (1973)) and the Love number h_2. (h_3 is also required for some minor lunar components of the generating potential.) The ocean tide ζ_o is more problematic. There are a number of numerical models of ζ_o available; none is completely satisfactory, and, in fact, the improvement of our knowledge of ζ_o is a major goal of altimetry. Probably the best current model of ζ_o for the deep-ocean regions is that computed at the Naval Surface Weapons Center (NSWC) by *Schwiderski* (1980, 1983); this model tide is provided on the GEOSAT geophysical data records as a standard tide correction for the altimetry. The load tide ζ_l is a measure of the deformation of the solid Earth under the weight of the ocean tide. ζ_l as presented below corresponds to (is, in fact, derived from) the NSWC ocean tide.

Direct tidal analysis of satellite altimetry is already promising to improve our knowledge of the ocean tide (*Cartwright & Ray*, 1989). In tidal analysis

of altimetry, it is usually more direct to derive an "altimetric tide" ζ_a, which is neither a geocentric tide nor a land-relative ocean tide but is given by

$$\zeta_a = \zeta_g - \zeta_b = \zeta_o + \zeta_l.$$

There are several points to make here. If the goal is simply to provide accurate tidal corrections to the altimetry so that other, more subtle oceanographic signals may be studied, ζ_a is actually what is required. If only ζ_o is available, as is the case for current GEOSAT data processing, then ζ_l must be computed to form ζ_a. But in addition to this use, knowledge of ζ_l in its own right has several applications. Among these are: (a) to compare the satellite tide ζ_a with tide gauges which are direct measurements of ζ_o; (b) to calibrate an altimeter by using local observations of sea level; (c) to compute ζ_o from ζ_a in order to provide corrections for Earth-tide measurements of gravity, tilt, and strain (*Harrison*, 1985); and (d) as a specific application, to estimate the loading tide contribution to the ζ_a(GEOSAT)$-\zeta_o$(NSWC) difference maps of *Cartwright & Ray* (1989).

The usual procedure for computing tidal loading effects for Earth-tide observations is to integrate the ocean tide over the surface of the globe using a numerical Green's function, as in the classic studies by *Longman* (1963) and *Farrell* (1972). This integration is moderately time consuming, but since there are normally only a few Earth-tide stations, the time is of little concern. For satellite altimetry, however, this is no longer the case, since the load must be evaluated at very nearly the same resolution as the ocean tide, which is $1° \times 1°$ for the current NSWC model. Efficient methods are therefore required. Thus, our secondary motivation in this work has been to experiment with the applicability of replacing the Green's function methodology with one based on a high-degree-and-order spherical harmonic expansion. This has allowed us to exploit recent advances in algorithm design for "fast" transforms.

The atlas of computed load-tide charts is presented in Appendix C. A previous suite of global loading maps was published by *Parke & Hendershott* (1980) and *Parke* (1982). Their maps are derived from their own ocean-tide model, which has somewhat fewer constituents and lower spatial resolution than the NSWC model. Quite recently, *Francis* (1989) has presented results similar to our own by a different method.

2 Formalism

In this section, let the tide ζ be a complex number whose real and imaginary parts are the in-phase and quadrature parts of a particular tidal constituent. Similarly, let U be a complex potential.

We will now briefly recapitulate the formalism for loading tide calculations. The theory is standard (e.g., *Lambeck*, 1988), but it is useful to have it summarized. The starting point, following *Munk & MacDonald* (1960), is to write the radial deformation ζ_l as a combination of loading Love numbers that are *defined* by

$$\zeta_l = \sum_n h'_n U'_n / g, \tag{1}$$

where U'_n is the n-th degree spherical harmonic component of the potential U' caused by the mass of the ocean tide ζ_o. For a spherical Earth of radius $a_e \gg \zeta_o$, U' is given by

$$U'(\theta,\phi) = G\rho_w a_e^2 \iint \frac{\zeta_o(\theta',\phi')}{r}\, d\Omega'$$

with ρ_w the density of seawater. r is the distance between (θ,ϕ) and (θ',ϕ') and, as usual, may be expressed as

$$\frac{1}{r} = \frac{1}{2a_e \sin\psi/2} = \frac{1}{a_e}\sum_{n=0}^{\infty} P_n(\cos\psi) \tag{2}$$

and, by the addition theorem, as

$$\frac{1}{r} = \frac{1}{a_e}\sum_{n=0}^{\infty}\sum_{m=-n}^{n} \frac{4\pi}{2n+1} Y^*_{nm}(\theta',\phi')\, Y_{nm}(\theta,\phi),$$

where the Y_{nm} are normalized, complex spherical harmonics. The tide ζ_o may be expressed in spherical harmonics:

$$\zeta_o(\theta,\phi) = \sum_{n=0}^{\infty}\sum_{m=-n}^{n} a_{nm} Y_{nm}(\theta,\phi) \tag{3}$$

where the coefficients are

$$a_{nm} = \iint Y^*_{nm}(\theta,\phi)\, \zeta_o(\theta,\phi)\, d\Omega, \tag{4}$$

which allows the potential to be expressed as

$$U'(\theta,\phi) = 4\pi G\rho_w a_e \sum_{n=0}^{\infty}\sum_{m=-n}^{n} \frac{a_{nm}}{2n+1} Y_{nm}(\theta,\phi). \tag{5}$$

The loading tide may now be expressed in two alternative ways. Combining (1) and (5) gives

$$\zeta_l(\theta,\phi) = \frac{\rho_w}{\rho_e}\sum_{n=0}^{\infty}\sum_{m=-n}^{n} \frac{3h'_n}{2n+1} a_{nm} Y_{nm}(\theta,\phi) \tag{6}$$

with ρ_e the mean density of the Earth. Alternatively, combining (1) and (2) gives

$$\zeta_l(\theta,\phi) = \rho_w a_e^2 \iint \zeta_o(\theta',\phi')\, \mathcal{G}(\psi)\, d\Omega' \tag{7}$$

where

$$\mathcal{G}(\psi) = \frac{a_e}{M_e}\sum_{n=0}^{\infty} h'_n\, P_n(\cos\psi) \tag{8}$$

and M_e is the mass of the Earth.

The two approaches (6) and (7) may be loosely described as the "wavenumber domain" and "space domain" approaches, respectively. In the past, both approaches have been used for computing loading corrections for various Earth-tide measurements, where, depending on the measurement type, the "operator" $3h'_n/2n+1$ or the Green's function $\mathcal{G}(\psi)$ is modified as required. Workers who have used the wavenumber domain for loading calculations include *Pertsev* (1966), *Groten & Brennecke* (1973), and *Goad* (1980). Nonetheless, more success has been achieved using (7) rather than (6), the primary reasons being efficiency and complications related to slow convergence of the series. The series (3) converges relatively slowly, which requires the maximum degree, say N, of the series to be large and thus the number of coefficients a_{nm}, evaluated by the surface integrals (4), to be quite high. On the other hand, after the function $\mathcal{G}(\psi)$ has been tabulated, (7) requires the evaluation of only one surface integral at each Earth-tide station. In our present application, however, we require ζ_l to be evaluated over the entire globe (or at least, over all the oceans). Below, we describe some algorithms that allow the summations in (3) and the discrete version of (4) to be carried out efficiently for large N (for 1° resolution, $N = 180$ is appropriate). The

result is that approach (6) will be found to be much more economical than (7) for our present application.

Furthermore, computing the loading effects of radial deformation is much more amenable to the use of spherical harmonics than computing any of the other quantities normally required in Earth-tide studies. The operator $3h'_n/2n+1$ in (6) ensures that the series for ζ_l converges faster than the series for ζ_o. In contrast, the operator to compute loading corrections for gravity is

$$\frac{n + 2h'_n - (n+1)k'_n}{2n+1} \tag{9}$$

which causes the series for gravity to converge no faster than the series for ζ_o, even allowing for the fact that the Love number k'_n decays as $\sim 1/n$ (see, however, the modification of (9) due to *Merriam* (1980)). The operators for tidal tilt and strain are worse yet, causing convergence more slowly than that for ζ_o. We may therefore expect that the spherical harmonic approach to quantities other than radial deformation may be less successful, although we have done no further investigation of the matter.

2.1 Spherical harmonics and fast transforms

When progressing from two-dimensional Fourier series on a rectangle to spherical harmonics on a sphere, it must seem a natural extension to attempt to incorporate the fast Fourier transform (FFT) algorithm. The matter has been studied by a number of authors since *Ricardi & Burrows* (1972), but the extension is only partially successful. Useful summaries are by *Swarztrauber* (1979) and *Colombo* (1981). As they note, it is clear that, during evaluation of the coefficients a_{nm} of (4), the integration over ϕ can be handled by an FFT. There exists, however, no fast Legendre transform for the integration over θ, so at this point a number of methods have been proposed. Some authors (e.g., *Brown*, 1985) have simply performed standard numerical quadratures for the Legendre transforms; others (e.g., *Dilts*, 1985) have expressed the Legendre functions as Fourier series so that a second FFT could be invoked; other approaches have been used as well. As *Colombo* (1981) has noted, the most efficient methods require $\mathcal{O}(N^3 \log N)$ arithmetic operations compared to $\mathcal{O}(N^4)$ operations for straightforward quadrature of (4). (For comparison, Fourier analysis on an $N \times N$ square requires but $\mathcal{O}(N^2 \log N)$

operations.)

The procedures we have used in our loading calculations are based on the work of *Swarztrauber* (1979) (see also *Browning et al.*, 1989). He uses an auxiliary coefficient function $Z_n^m(\theta)$ which allows the harmonic coefficients to be computed by

$$a_{nm} = \sum_{j=1}^{2N} \sum_{i=1}^{N} Z_n^m(\theta_i)\zeta_o(\theta_i, \phi_j)\, e^{im\phi}.$$

The functions Z_n^m for spherical harmonic analysis thus correspond to the Legendre functions P_n^m for spherical harmonic synthesis. The reader may consult the references for further details.

3 Accuracy Assessments

We divide our discussion on the accuracy of the loading tide calculations into two sections. The first concerns the computational method: spherical harmonics vs. Green's functions. The second section concerns a more general assessment independent of the computational method.

3.1 Comparisons over the Indian Ocean

This section reports on some comparisons of the spherical harmonic and Green's function approaches to ocean loading calculations of radial deformation. This testing is important for several reasons. Firstly, even though we are using a high-degree spherical harmonic series ($N = 180$), it is important to establish that this is indeed high enough. After all, *Farrell* (1972) used $N = 10000$ for evaluating his Green's function using the series (8). Secondly, it is natural to expect certain manifestations of the Gibbs' phenomenon—at least in the synthesis of ζ_o by (3)—particularly near coastal areas where the ocean tide jumps discontinuously from a possibly large value to zero over land. The effect of this on the radial deformation must be monitored.

In Figures 1, 2, and 3 are shown the results of three loading tide computations for the M_2 constituent in the Indian Ocean area, derived from the (global) M_2 model of *Schwiderski* (1983). Figure 1 was computed using the Green's function tabulated by *Farrell* (1972) for the Gutenberg-Bullen Earth model. (Some further details of this are given in Appendix A.) Figures 2 and

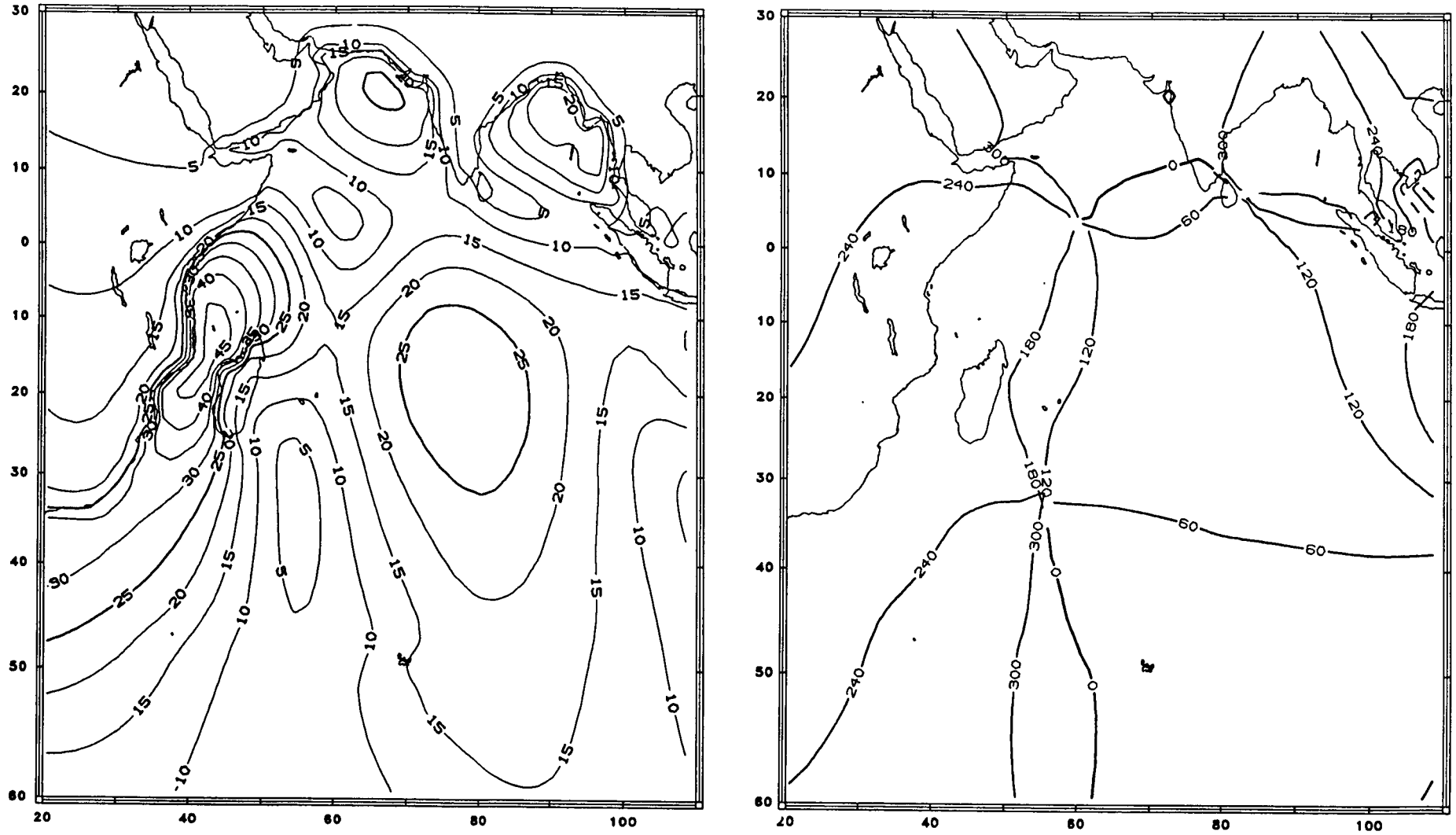

Figure 1: Maps of the M_2 load tide, using Farrell's Green's function. Amplitude contour interval 5 mm; Greenwich phases every 60°.

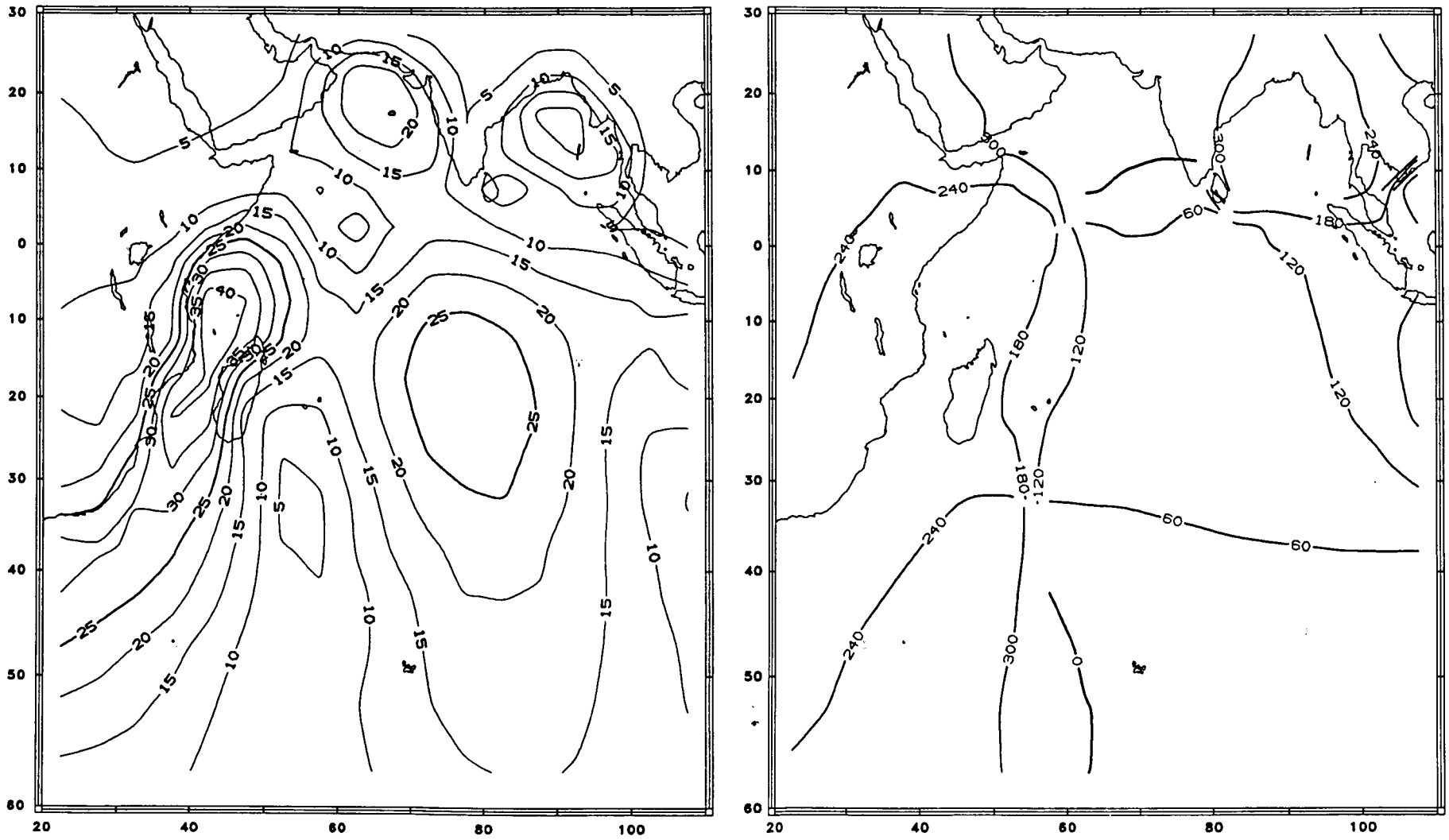

Figure 2: Maps of the M_2 load tide, using spherical harmonics with $N = 36$.

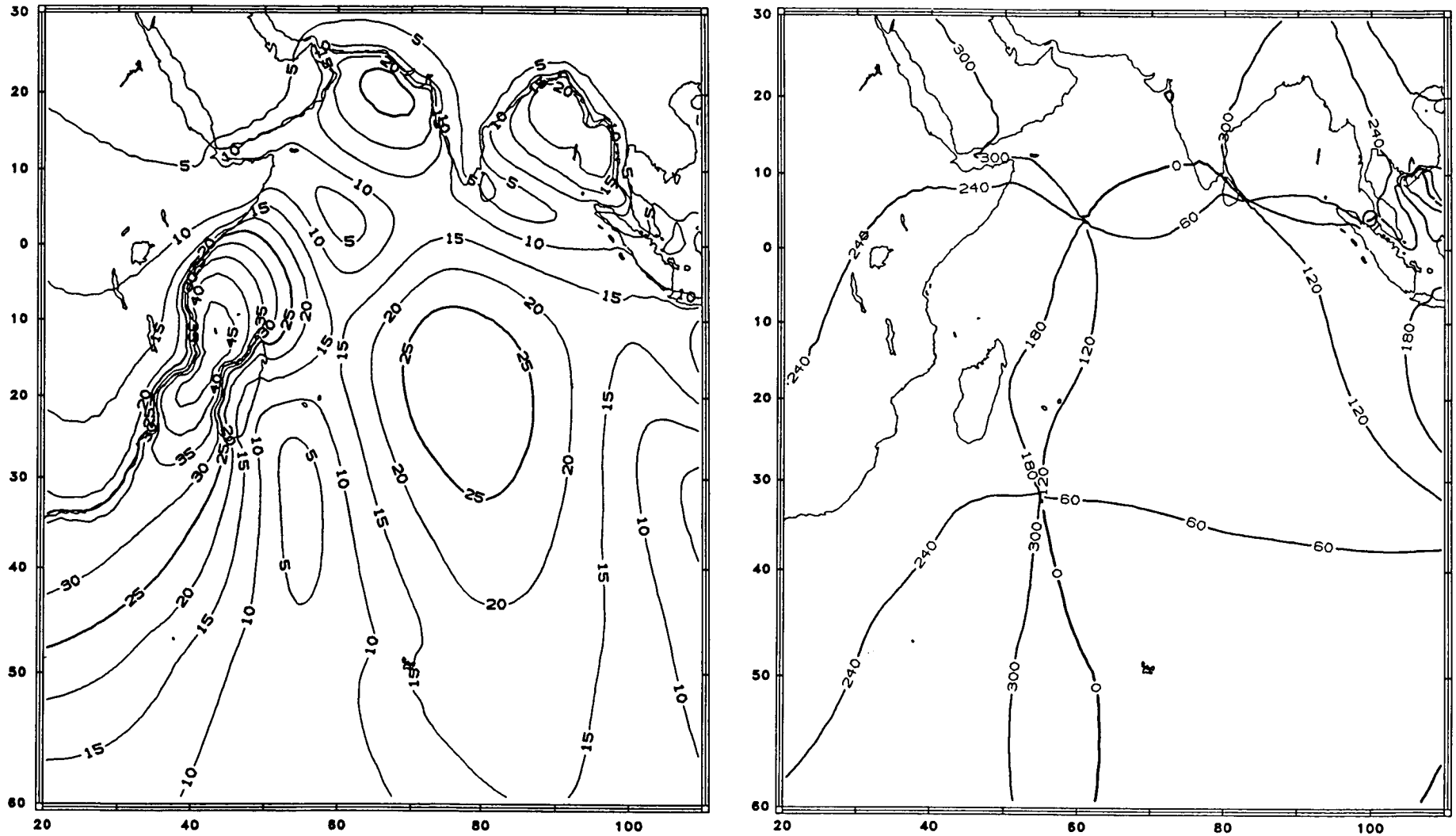

Figure 3: Maps of the M_2 load tide, using spherical harmonics with $N = 180$.

3 show the results of the spherical harmonic series approach, with $N = 36$ and $N = 180$, respectively, using the Gutenberg-Bullen Love numbers h'_n also tabulated by *Farrell* (1972).

From Figure 2 it is apparent that the resolution provided at $N = 36$ is too coarse, even though the large-scale structure is probably adequate. The agreement between Figures 1 and 3 is quite remarkable, and establishes the validity of the spherical harmonic approach. Although there is some "wiggliness" in the contours over Africa in Figure 3, they are of no consequence; most importantly, there is no serious indication of any Gibbs-type ringing, even near Madagascar where the NSWC tide is over 1 m in amplitude.

Figure 3 (as well as Figure 2) was actually part of a global calculation—it in fact is a portion of the global Figures C5–6 of Appendix C. To produce this global figure required almost exactly 10 times less computer-time than did Figure 1, which was computed only for the area shown in the figure.

3.2 General accuracy assessments

The previous section established the accuracy of the spherical harmonic calculation of radial deformation by comparing it to the standard Green's function calculation. There are several other issues that affect accuracy that are independent of the spherical harmonic/Green's function choice.

Ocean tide model. The most obvious issue concerns the accuracy of the ocean tide ζ_o—in our case, the NSWC numerical model. The NSWC M_2 model is advertised as accurate to better than 5 cm anywhere in the open ocean (*Schwiderski*, 1983). A recent comparison of the M_2 model with 66 open ocean (island or bottom pressure) measurements shows a standard deviation of 4.2 cm (*Cartwright & Ray*, 1989), which would indicate the 5-cm limit is often exceeded. In certain locations the model is known to be inaccurate due to lack of real data. Nevertheless, as noted below, a comparison between our load tide maps (Appendix C) and the Parke-Hendershott (1980; Fig. 13) load tide maps shows good agreement, almost always within 1 cm—and a large fraction of that must be due to errors in the Parke-Hendershott ocean tide. This fact, and the 7% rule of thumb (i.e., $\zeta_l \approx -0.07\zeta_o$, see below), would indicate that a reasonable estimate of the loading error due to errors in the ocean tide is 0.5 cm (in the open ocean).

In coastal and shelf areas, of course, the NSWC model is generally poor because the 1° resolution is too coarse to model such complex tides. Therefore, our corresponding load tide maps are likewise suspect in these areas. For accurate loading computations in such areas, the standard recourse (e.g., *Baker*, 1980) is to complement the open-ocean tide model with a local, high-resolution model. This proviso is particularly relevant to VLBI measurements from antennae located in coastal areas like, for example, the Gulf of Alaska.

Mass conservation. In theory any model of the ocean tide should conserve mass. In the spherical harmonic decomposition (3) we should then have $a_{00} = 0$. For a variety of reasons, however, most numerical models of the tides violate this constraint, and some controversy has developed on how best to allow for this. The degree of non-conservation for the NSWC model may be seen in the list of spherical harmonic coefficients tabulated in Appendix B.

Farrell (1972b) has stressed the need for forcing mass conservation in the ocean model to improve the residuals of gravity tides, although (in *Farrell*, 1973) he reports that doing so by (a) removing a (complex) slab of water from the model or (b) forcing $a_{00} = 0$ gave similar results for the perturbed potential, an issue later clarified by *Agnew* (1983). We observed that supplementing Farrell's set of Love numbers (which had no $n = 0$ term) with $h'_0 = -0.134$ from *Longman* (1963) results simply in a (bias) shift of ζ_l by $0.34 - 0.23i$ mm. This, as well as the 7% rule applied to the a_{00} terms of Appendix B, leads us to believe that mass non-conservation in the NSWC model is of little concern for our deformation calculations.

Earth models. If we compare the load tide results for M_2 as given in the atlas with similar calculations that use the Love numbers of Pertsev & Ivanov (tabulated in *Melchior*, 1983) as well as of *Zschau* (1978), we find maximum vector differences of 1.39 and 1.42 mm, respectively, of which about 30% is due to the simple $n = 0$ bias term. We conclude that the choice of the gross, radially symmetric, frequency-independent Earth model is of little concern.

Of more concern, however, may be lateral heterogeneities of the Earth that are not included in the Earth models. Effects of local geology or topography, for example, are known to play a large role—as much as 50% or more (*Farrell*, 1979)—in Earth-tide observations of tilt and strain, less so

for gravity. The effect was first noticed when scientists compared nearby observations that were unexpectedly discordant. Radial deformation is not (as of yet) directly measured at the required precision, so the effects of lateral heterogeneities on it are not completely evident. Finite element modeling, however, by *Gong et al.* (1975) and *Beaumont* (1978) indicate that effects larger than 10% are possible. In light of this, our maps should be interpreted as the "homogeneous" load tide, following the terminology of *Berger & Beaumont* (1976).

We should also point out that, even though it is easily incorporated into the spherical-harmonic methodology, we have not allowed for any frequency dependence in the Love numbers. In particular, the nearly-diurnal free wobble, due to the liquid outer core, affects the diurnal band near our K_1 constituent by increasing h'_n for the $(n,m) = (2,1)$ harmonic only (*Wahr & Sasao*, 1981). (Resonance effects on the ocean model can be assumed to be incorporated automatically by the model's observational constraints.) From Wahr & Sasao's Table 5, the effect is seen to be less than 1% of the body tide for K_1, which, at this level, we may neglect.

4 Discussion

Appendix C presents an atlas of maps showing the amplitudes and Greenwich phases for the load tides corresponding to all but one constituent of the NSWC ocean model—namely the semidiurnals K_2, S_2, M_2, N_2, the diurnals K_1, P_1, O_1, Q_1, and the long-period tides M_f and M_m. All were computed using the Gutenberg-Bullen Love numbers (with no frequency dependence) as tabulated by *Farrell* (1972). (The NSWC model also includes the semiannual S_{sa} tide. We have not included load-tide maps for S_{sa}, since this component is influenced by large thermal and atmospheric effects that do not load the lithosphere.)

The general features of the maps are in good agreement with the 6 charts previously published by *Parke & Hendershott* (1980) and *Parke* (1982), although, as one would expect, many of the details are different. In general, for the semidiurnal tides, the Parke-Hendershott amplitudes are slightly larger than our amplitudes, the largest discrepancy being nearly 10 mm in the M_2 tide for the high-amplitude region in the Indian Ocean. This arises because

the Parke-Hendershott ocean tide there is nearly 10 cm larger than the NSWC tide.

For the important M_2 constituent, we have converted the amplitude and phase plots to in-phase and quadrature components (i.e., $H \cos G$ and $H \sin G$). This is for direct comparison to the ζ_a(GEOSAT)$-\zeta_o$(NSWC) (color) difference maps of *Cartwright & Ray* (1989) and allows us to estimate the contribution of the load tide to this difference. These plots are shown in Figures 4 and 5. Comparing these to the Cartwright/Ray maps shows little similarity. Furthermore, the small amplitudes of the load tide—4 cm or less—would not markedly change the (GEOSAT−NSWC) discrepancy areas. One region of correlation is the large quadrature anomaly off the coast of northeastern Brazil; but the 3-cm load tide still leaves a (GEOSAT−NSWC) difference of nearly 15 cm.

4.1 Coherence of ocean and load tides

Various tidal authorities (e.g. *Schwiderski*, 1983) have used in the past the following rule-of-thumb for estimating the load tide ζ_l from the land-relative ocean tide ζ_o:

$$\zeta_l = -\epsilon \zeta_o$$

with ϵ typically around 0.07—thus, the "7% rule" referred to earlier in this work.

Such a rule is obviously but a rough approximation. To see the extent of the approximation, we have computed the coherence between the NSWC ocean tides and the load tides of Appendix C for a number of constituents. The coherence is given by (with ζ complex)

$$\gamma^2 = \frac{|\langle \zeta_o^* \zeta_l \rangle|^2}{\langle \zeta_o^* \zeta_o \rangle \langle \zeta_l^* \zeta_l \rangle}$$

where $\langle\ \rangle$ denotes averaging over the global ocean. The results are summarized in Table 1, along with the least-squares estimates of ϵ. ϵ is shown as a real number; allowing it to be complex gives an insignificant imaginary component. All the ϵ estimates for the short-period tides are less than 7%. Performing the calculations only over the deep (> 1 km) ocean improves γ^2 marginally and increases ϵ at most ten percent.

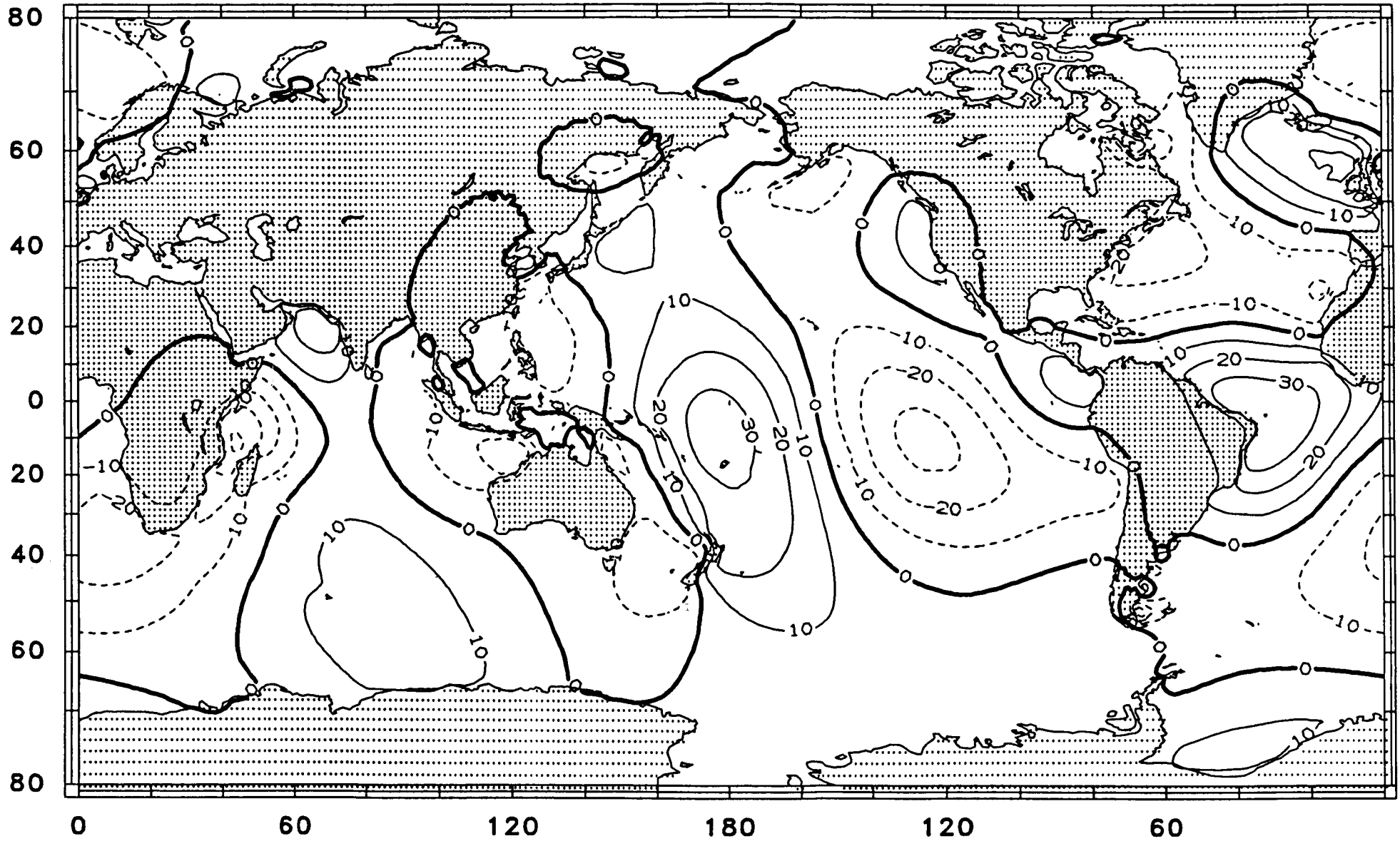

Figure 4: In-phase component of the M_2 load tide, in mm.

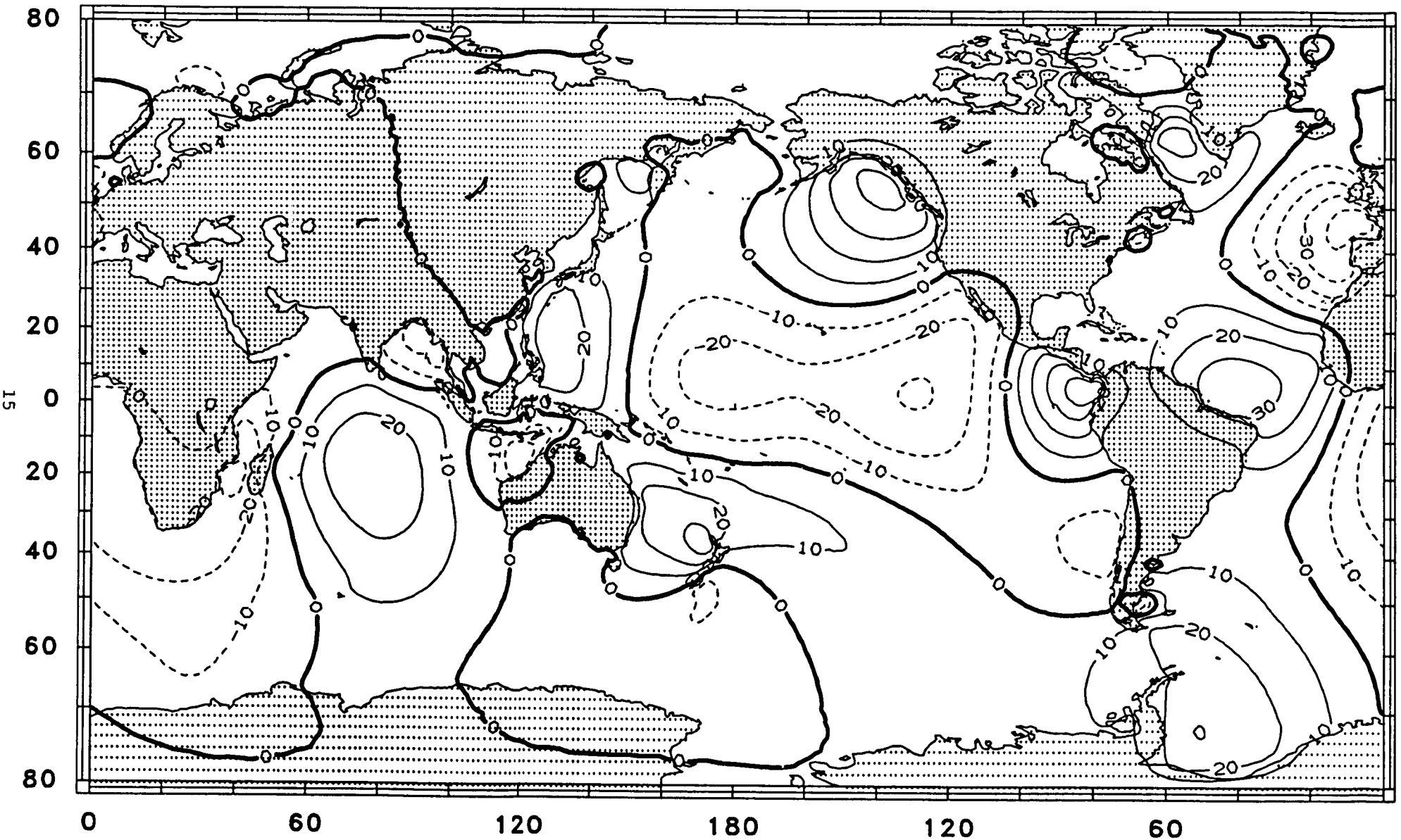

Figure 5: Quadrature component of the M_2 load tide, in mm.

Table 1: Coherence and scaling coefficients.

Tide	γ^2	$\hat{\epsilon}$
M_2	0.84	0.047
S_2	0.86	0.046
K_1	0.83	0.057
O_1	0.87	0.062
M_f	0.94	0.078
M_m	0.86	0.066

In Table 1, the ϵ-values for the short-period tides agree almost exactly with similar values computed by *Parke* (1982) for the Parke-Hendershott ocean tide, except for K_1, which is here somewhat smaller. These values of ϵ are not comparable with the larger values of *Accad & Pekeris* (1978), since they include (in their variable K) effects of ocean self-attraction, which do not concern us here.

Finally, to show even more plainly the limitations of this "7% rule," we have used our Appendix C maps to compute the vector error in the approximation for $\epsilon = 0.0667$ (the value used by *Schwiderski* (1983)). This is shown as Figure 6. (*Francis* (1989) has recently computed a similar map, with nearly identical results.) The errors are clearly largest near coastlines; in the Gulf of Alaska, for example, the error in near 100%. Figure 7 shows the errors when $\epsilon = 0.047$. The large errors near coastlines are somewhat reduced, at the expense of increased errors in the open ocean where they tend to mimic the amplitudes of ζ_l shown in Figure C5, indicative of ϵ being too small. The error in the mid-Pacific approaches 15 mm—nearly 50% of ζ_l.

Acknowledgments: Part of our software was originally written by Paul N. Swarztrauber and John C. Adams of the National Center for Atmospheric Research, Boulder. We thank Oscar L. Colombo and David E. Cartwright for many useful discussions. This work was funded by the NASA TOPEX/POSEIDON Project.

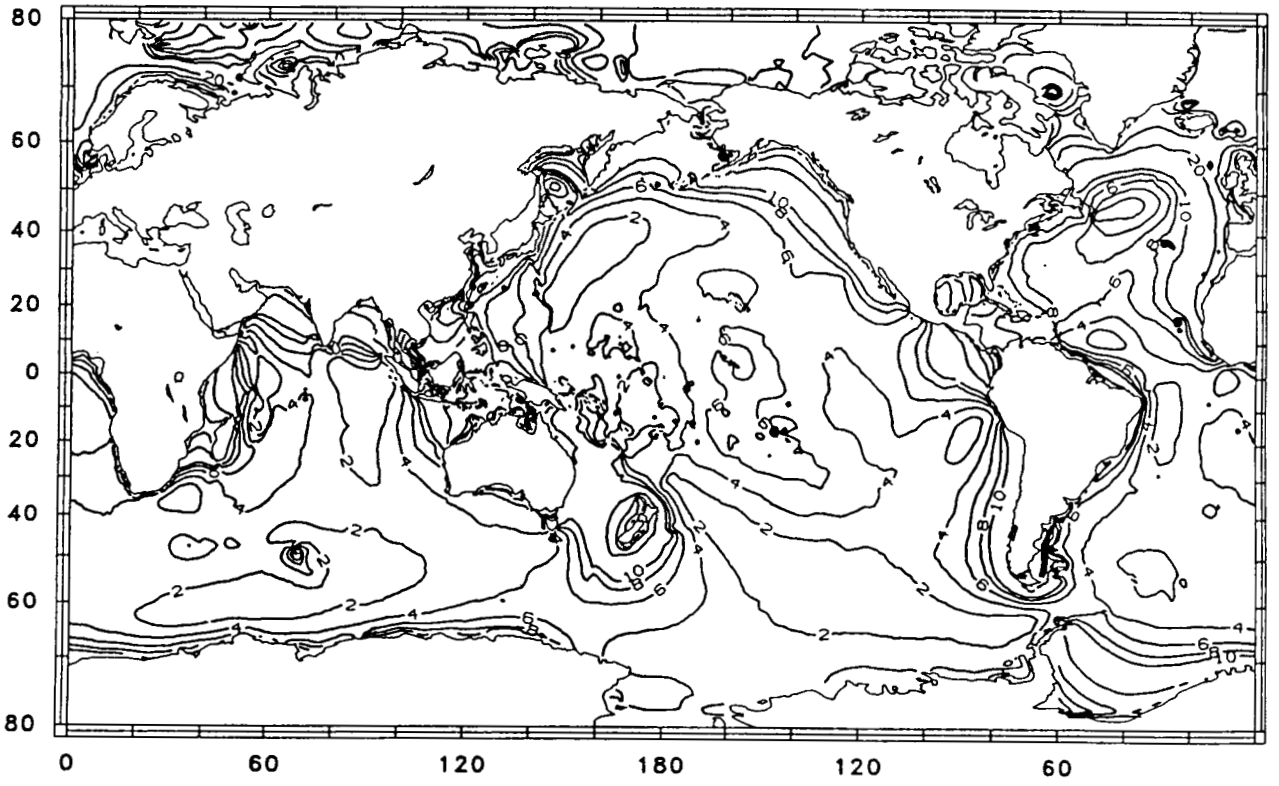

Figure 6: Vector error in the M_2 load tide when assuming $\zeta_l = -0.0667\zeta_o$, in mm.

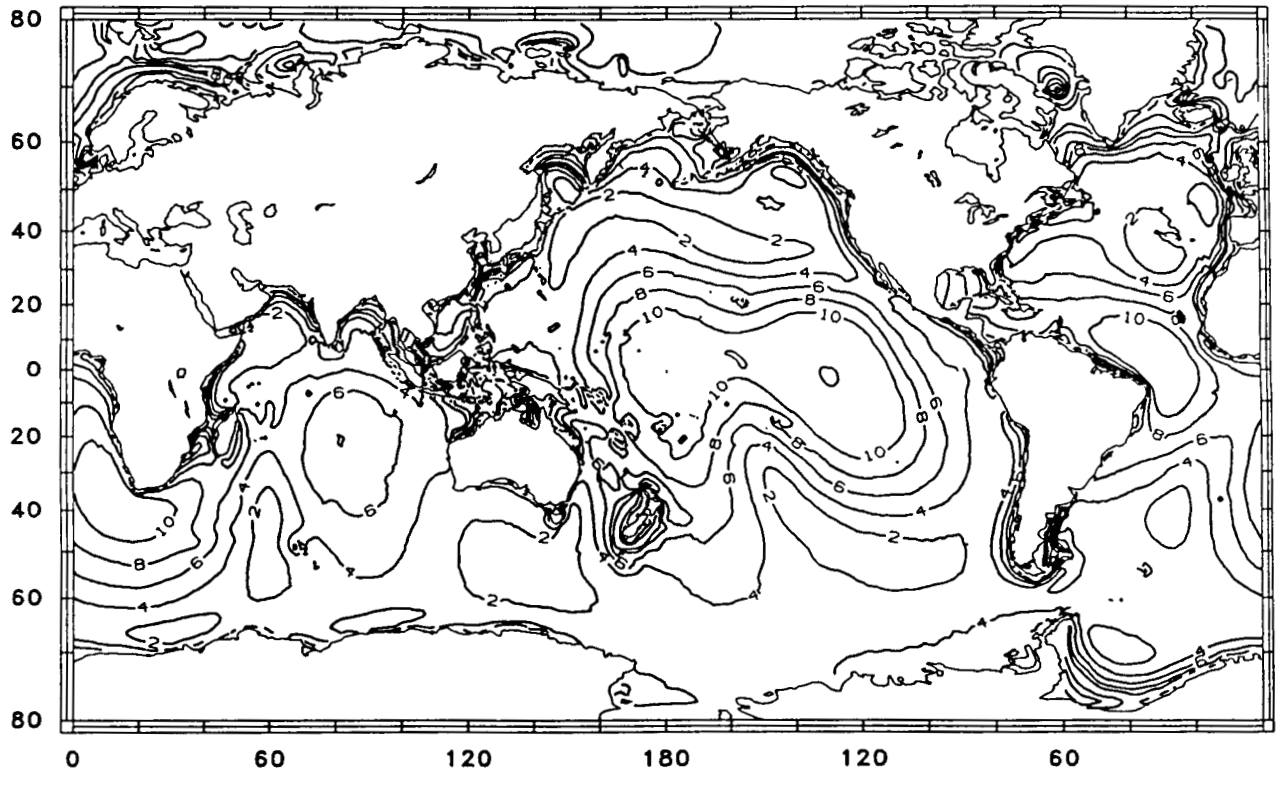

Figure 7: Vector error in the M_2 load tide when assuming $\zeta_l = -0.047\zeta_o$. Contour lines at 2, 4, 6, 8, 10, 15, 20, 30, 40 mm.

REFERENCES

Accad, Y. and C. L. Pekeris, Solution of the tidal equations for the M_2 and S_2 tides in the world oceans from a knowledge of the tidal potential alone, *Phil. Trans. R. Soc., London*, **290**, 235–266, 1978.

Agnew, D. C., Conservation of mass in tidal loading computations, *Geophys. J. R. astr. Soc.*, **72**, 321–325, 1983.

Baker, T. F., Tidal gravity in Britain: tidal loading and the spatial distribution of the marine tide, *Geophys. J. R. astr. Soc.*, **62**, 249–267, 1980.

Baker, T. F., Tidal deformations of the Earth, *Sci. Prog.*, **69**, 197–233, 1984.

Beaumont, C., Tidal loading: crustal structure of Nova Scotia and the M_2 tide in the northwest Atlantic from tilt and gravity observations, *Geophys. J. R. astr. Soc.*, **53**, 27–53, 1978.

Berger, J. and C. Beaumont, An analysis of tidal strain from the United States of America. II: the inhomogeneous tide, *Bull., Seis. Soc. Am.*, **66**, 1821–1846, 1976.

Born, G. H., C. Wunsch, and C. A. Yamarone, TOPEX: Observing the oceans from space, EOS, *Trans. Am. Geophys. Union*, **65**, 433-434, 1984.

Brown, T. M., Solar rotation as a function of depth and latitude, *Nature*, **317**, 591–594, 1985.

Browning, G. L., J. J. Hack, and P. N. Swarztrauber, A comparison of three numerical methods for solving differential equations on the sphere, *Mon. Weather Rev.*, in press, 1989.

Cartwright, D. E. and A. C. Edden, Corrected tables of tidal harmonics, *Geophys. J. R. astr. Soc.*, **33**, 253–264, 1973.

Cartwright, D. E. and R. D. Ray, Oceanic tides from GEOSAT-ERM altimetry, submitted for publication, 1989.

Colombo, O., Numerical methods for harmonic analysis on the sphere, Ohio State Univ. Dept. Geodetic Sci. Rep. 310, Columbus, 1981.

Dilts, G. A., Computation of spherical harmonic expansion coefficients via FFT's, *J. Comput. Phys.*, **57**, 439–453, 1985.

Farrell, W. E., Deformation of the Earth by surface loads, *Rev. Geophys. Space Phys.*, **10**, 761–797, 1972.

Farrell, W. E., Global calculations of tidal loading, *Nature Phys. Sci.*, **238**, 43–44, 1972b.

Farrell, W. E., Earth tides, ocean tides, and tidal loading, *Phil. Trans. R. Soc., London*, **A274**, 253–259, 1973.

Farrell, W. E., Earth tides, *Rev. Geophys. Space Phys.*, **17**, 1442–1446, 1979.

Francis, O., Global charts of ocean tides loading effects, Meeting of Topex/Pos. Sci. Working Team, Pasadena, 1989.

Goad, C., The computation of tidal loading effects with integrated Green's functions, 2nd Intern. Sym., Problems Related to the Redefinition of North American Vertical Geodetic Networks, *Proceedings*, Ottawa, 587–601, 1980.

Gong, C., R. C. Jachens, and J. T. Kuo, A pseudo three-dimensional finite element formulation for elastostatic problems and its geophysical applications, *J. Geophys. Res.*, **80**, 4103–4110, 1975.

Groten, E. and J. Brennecke, Global interaction between earth and sea tides, *J. Geophys. Res.*, **78**, 8519–8526, 1973.

Harrison J. C. (ed.), *Earth Tides*, Van Nostrand Reinhold Co., New York, 1985.

Lambeck, K. *Geophysical Geodesy*, Oxford Univ. Press, 1988.

Longman, I. M., A Green's function for determining the deformation of the Earth under surface mass loads, 2, *J. Geophys. Res.*, **68**, 485–496, 1963.

Melchior, P., *The Tides of the Planet Earth*, Pergamon Press, Oxford, 1983.

Merriam, J. B., The series computation of the gravitational perturbation due to an ocean tide, *Phys. Earth Planet. Inter.*, **23**, 81–86, 1980.

Munk, W. H. and G. J. F. MacDonald, *The Rotation of the Earth*, Cambridge Univ. Press, Cambridge, 1960.

Parke, M. E., O_1, P_1, N_2 models of the global ocean tide on an elastic Earth plus surface potential and spherical harmonic decompositions for M_2, S_2, and K_1, *Marine Geodesy*, **6**, 35–81, 1982.

Parke, M. E. and M. C. Hendershott, M_2, S_2, K_1 models of the global ocean tide

on an elastic earth, *Marine Geodesy*, **3**, 379–407, 1980.

Pertsev, B. P., On the effect of ocean tides on tidal variations of gravity (Engl. transl.), *Izvest., Phys. Solid Earth*, 636–639, Oct. 1966.

Ricardi L. J. and J. L. Burrows, A recurrence technique for expanding a function in spherical harmonics, *IEEE Trans. Comput.*, **C-21**, 583–585, 1972.

Schwiderski, E. W., Ocean tides: I—Global ocean tidal equations; II—A hydrodynamic interpolation model, *Marine Geodesy*, **3**, 161–217 and 219–255, 1980.

Schwiderski, E. W., Atlas of ocean tidal charts and maps. I: the semidiurnal principal lunar tide M_2, *Marine Geodesy*, **6**, 219–265, 1983.

Swarztrauber, P. N., On the spectral approximation of discrete scalar and vector functions on the sphere, *SIAM J. Numer. Anal.*, **16**, 934–949, 1979.

van Dooren, P. and L. de Ridder, An adaptive algorithm for numerical integration over an n-dimensional cube, *J. Comput. Appl. Math.*, **2**, 207–217, 1976.

Wahr, J. M. and T. Sasao, A diurnal resonance in the ocean tide and in the Earth's load response due to the resonant free 'core nutation', *Geophys. J. R. astr. Soc.*, **64**, 747–765, 1981.

Zschau, J., Tidal friction in the solid Earth: loading tides versus body tides, in *Tidal Friction and the Earth's Rotation*, Springer-Verlag, New York, 1978.

Appendix A Integrating Green's Functions

We discuss in this appendix a few details concerning the calculation of loading tides with a (numerical) Green's function.

The loading tide, given by Eq. (7), is discretized as follows:

$$\begin{aligned} \zeta_l(\theta,\phi) &= \rho_w a_e^2 \iint_\Omega \zeta_o(\theta',\phi')\, \mathcal{G}(\psi)\, d\Omega' \\ &= \rho_w a_e^2 \sum_i \zeta_{oi} \iint_{\Omega_i} \mathcal{G}(\psi)\, d\Omega', \end{aligned} \tag{A1}$$

since the ocean tide ζ_o is a constant over each $1^\circ \times 1^\circ$ block Ω_i. The Green's function $\mathcal{G}(\psi)$ for radial deformation has an (integrable) $1/\psi$ singularity as $\psi \to 0$ (*Farrell*, 1972), which complicates evaluation of the integral in (A1). However, when ψ is sufficiently large, the integral can be approximated using the centroid rule

$$\iint_{\Omega_i} \mathcal{G}(\psi)\, d\Omega' = \mathcal{G}(\psi_i)\ \Delta\Omega_i = \mathcal{G}(\psi_i) \sin\theta_i' \,\Delta\theta_i' \,\Delta\phi_i'$$

where ψ_i is the distance from (θ,ϕ) to the center of Ω_i and $\Delta\Omega_i$ is the solid angle subtended by Ω_i. Numerical tests indicate this approximation yields an error typically no more than 5% when $\psi \geq 1^\circ$ and no more than 1% when $\psi \geq 5^\circ$.

For the blocks Ω_i in the immediate neighborhood of the computation point (θ,ϕ), a more accurate integration rule must be used. We have used for this region an adaptive quadrature algorithm due to *van Dooren & de Ridder* (1976). This algorithm does not require the evaluation of the integrand on the boundary of the region, and it can therefore handle a singularity there. Thus for the block Ω_i which contains the point (θ,ϕ) where $\psi = 0$, we split the block into two regions with (θ,ϕ) on the boundary and integrate the two regions separately.

Calculations of the contribution of individual regions to the summation in (A1) as a function of ψ shows a quite complex and unpredictable behavior, due to the complicated behavior of the tides. It is therefore essential to carry out the integration over the entire globe even though $\mathcal{G}(\psi)$ decays rapidly away from the origin.

Appendix B Tide Coefficients

As a by-product of our spherical harmonic analyses of the NSWC ocean tide models, we list here the first few harmonic coefficients for each constituent. They may be of some interest in their own right. To interpret them, however, requires knowledge of the normalization, and it seems nearly everyone differs in this regard. As noted elsewhere, we have used a procedure due to Swarztrauber, who expresses a spherical harmonic series as (all quantities real)

$$\tfrac{1}{2}\sum_{n=0}^{N} a_{n0}P_n^0(\cos\theta) + \sum_{n=1}^{N}\sum_{m=1}^{n}(a_{nm}\cos m\phi - b_{nm}\sin m\phi)P_n^m(\cos\theta). \qquad \text{(B1)}$$

The normalization is set such that $P_n^m(\mu)$ is normalized when it (alone) is integrated from $\mu = -1$ to 1. Thus,

$$\iint_\Omega \left[P_n^m(\cos\theta)\left\{\begin{array}{c}\sin m\phi\\ \cos m\phi\end{array}\right\}\right]^2 d\Omega = \pi.$$

A particular tidal constituent $\zeta = H\cos(\sigma t - G)$ with speed σ and Greenwich phase G is decomposed into in-phase and quadrature components ζ_1 and ζ_2:

$$\zeta_1 = H\cos G \qquad \zeta_2 = H\sin G.$$

These components are then expanded in spherical harmonics:

$$\zeta_1 = \sum_{n=0}^{N}\sum_{m=0}^{n}{}'(a_{nm}\cos m\phi - b_{nm}\sin m\phi)\,P_n^m(\cos\theta)$$

$$\zeta_2 = \sum_{n=0}^{N}\sum_{m=0}^{n}{}'(c_{nm}\cos m\phi - d_{nm}\sin m\phi)\,P_n^m(\cos\theta)$$

where the prime on the second summation indicates that the first term is multiplied by 1/2, in agreement with (B1). The coefficients a_{nm}, b_{nm}, c_{nm}, and d_{nm} are listed in the following tables up to degree and order 6; units are millimeters.

To convert our tabulated coefficients to the more conventional notation used in satellite geodesy (e.g. *Lambeck*, 1988), use the following formulae:

$$\begin{aligned} D_{nm}^{\pm}\cos\varepsilon_{nm}^{\pm} &= \tfrac{1}{2}(a_{nm} \pm d_{nm})N_n^m \\ D_{nm}^{\pm}\sin\varepsilon_{nm}^{\pm} &= \tfrac{1}{2}(c_{nm} \mp b_{nm})N_n^m \end{aligned}$$

where the normalization factor is

$$N_n^m = \left[\frac{2n+1}{2}\frac{(n-m)!}{(n+m)!}\right]^{1/2}.$$

Coefficients of the NSWC tide K_2.

n	m	a_{nm}	b_{nm}	c_{nm}	d_{nm}
0	0	1.60		0.44	
1	0	0.60		0.78	
1	1	-0.73	2.04	3.51	0.99
2	0	4.88		-3.49	
2	1	-1.28	4.31	-1.49	0.43
2	2	-4.63	-3.88	7.74	-6.61
3	0	-2.31		-1.72	
3	1	-1.50	1.71	7.06	2.25
3	2	-1.82	4.30	-6.40	-1.24
3	3	2.88	-0.34	6.26	-6.06
4	0	-6.55		-1.76	
4	1	-4.50	-3.35	8.73	-3.29
4	2	10.05	3.41	-1.30	8.45
4	3	0.42	3.74	-4.00	12.70
4	4	-6.53	-8.69	-2.00	-8.06
5	0	0.01		8.58	
5	1	2.80	1.10	-15.35	-6.05
5	2	-6.89	-8.47	0.95	7.03
5	3	-5.94	3.87	4.06	-7.97
5	4	-5.67	-3.13	6.13	12.86
5	5	7.80	3.59	-6.08	-2.78
6	0	4.29		0.62	
6	1	0.86	0.55	-3.51	3.88
6	2	-6.41	-2.54	0.80	-8.05
6	3	-4.41	-1.55	-0.71	3.74
6	4	3.25	-2.86	0.18	-0.98
6	5	-3.81	7.26	2.34	-6.09
6	6	-5.85	-2.37	8.22	12.66

Coefficients of the NSWC tide S_2.

n	m	a_{nm}	b_{nm}	c_{nm}	d_{nm}
0	0	0.43		0.00	
1	0	2.28		2.68	
1	1	1.70	7.81	11.83	1.73
2	0	15.67		-11.66	
2	1	-5.00	14.67	-3.98	0.00
2	2	-20.51	-15.61	25.28	-20.52
3	0	0.04		-2.41	
3	1	-9.51	7.49	26.05	6.83
3	2	-9.73	10.23	-18.49	-2.41
3	3	17.77	-0.40	23.85	-28.22
4	0	-25.80		-8.62	
4	1	-15.06	-11.81	28.82	-6.84
4	2	37.08	11.25	-4.77	28.03
4	3	3.31	11.97	-21.28	47.82
4	4	-23.13	-29.29	-2.58	-32.37
5	0	-3.70		28.00	
5	1	7.77	1.27	-51.45	-25.80
5	2	-21.59	-30.43	3.11	24.03
5	3	-22.76	15.90	16.87	-28.51
5	4	-20.17	-15.55	23.71	46.81
5	5	29.29	13.54	-25.19	-6.81
6	0	16.16		7.81	
6	1	7.22	4.16	-11.97	12.56
6	2	-23.70	-9.26	2.04	-30.08
6	3	-14.06	-5.81	0.79	14.31
6	4	8.59	-8.71	1.52	-2.59
6	5	-11.50	26.61	8.95	-21.75
6	6	-18.10	-7.56	29.99	43.44

Coefficients of the NSWC tide M_2.

n	m	a_{nm}	b_{nm}	c_{nm}	d_{nm}
0	0	12.47		-6.61	
1	0	2.44		8.52	
1	1	24.88	19.41	4.70	-10.99
2	0	-2.15		-32.36	
2	1	-23.00	11.54	-10.81	-14.34
2	2	-55.29	-52.96	69.27	-82.67
3	0	38.58		-4.13	
3	1	36.52	30.38	80.40	-28.91
3	2	-3.45	37.29	-4.77	11.10
3	3	105.28	-43.79	70.35	-25.41
4	0	-61.01		5.28	
4	1	-5.53	-5.36	78.88	33.69
4	2	67.73	93.64	-12.51	79.04
4	3	-78.93	83.26	-66.25	66.79
4	4	-87.59	-59.71	21.81	-33.88
5	0	-23.53		21.49	
5	1	-62.35	-38.51	-121.65	-55.63
5	2	-82.80	-66.30	2.24	79.78
5	3	-31.22	-19.85	16.75	-65.78
5	4	15.60	-42.22	69.51	88.55
5	5	52.99	-24.78	-17.06	-47.47
6	0	69.30		11.32	
6	1	1.91	3.67	-35.55	0.63
6	2	-18.02	-61.49	53.70	-46.50
6	3	-24.71	-2.87	35.08	-1.64
6	4	22.66	0.94	43.30	24.15
6	5	-16.38	45.19	-3.43	-51.84
6	6	8.31	49.03	99.50	86.07

Coefficients of the NSWC tide N_2.

n	m	a_{nm}	b_{nm}	c_{nm}	d_{nm}
0	0	-0.43		-5.01	
1	0	2.76		0.49	
1	1	2.63	5.85	-0.37	-4.72
2	0	1.24		-0.27	
2	1	-7.55	-4.39	-2.09	-2.13
2	2	-7.25	-16.73	15.63	-17.33
3	0	7.68		-5.38	
3	1	11.31	7.10	12.00	-6.17
3	2	1.44	8.65	-4.12	0.11
3	3	26.67	-7.05	9.59	-3.88
4	0	-17.53		-0.74	
4	1	4.16	1.44	12.42	4.68
4	2	17.67	26.90	-3.67	5.47
4	3	-21.29	17.45	-3.98	10.50
4	4	-20.65	-12.24	10.72	-6.47
5	0	-5.38		10.48	
5	1	-19.72	-14.91	-17.03	-9.29
5	2	-19.43	-9.00	11.58	21.66
5	3	-7.81	-9.36	4.91	-11.85
5	4	8.68	-7.79	9.58	21.11
5	5	13.74	-12.81	-3.96	-5.81
6	0	18.15		-3.29	
6	1	-1.28	3.83	-7.17	0.69
6	2	0.27	-15.86	5.24	-4.62
6	3	-3.59	-1.06	6.09	3.06
6	4	10.71	4.72	8.79	4.75
6	5	-4.05	8.44	0.88	-10.77
6	6	7.46	14.51	19.87	12.70

Coefficients of the NSWC tide K_1.

n	m	a_{nm}	b_{nm}	c_{nm}	d_{nm}
0	0	1.78		0.39	
1	0	8.12		-36.66	
1	1	11.96	-8.78	3.30	-12.96
2	0	-10.65		-7.14	
2	1	-14.49	-45.37	17.19	-45.86
2	2	24.19	4.06	-2.08	34.60
3	0	13.31		19.44	
3	1	-12.71	4.67	32.31	30.56
3	2	4.77	23.63	3.34	48.50
3	3	-42.16	-47.46	-6.72	-45.04
4	0	2.42		14.12	
4	1	-51.19	23.56	2.62	-26.93
4	2	13.21	8.85	-17.41	5.79
4	3	-14.01	1.31	17.33	-29.29
4	4	10.78	47.99	14.71	17.99
5	0	-21.71		-11.15	
5	1	33.10	-6.51	-20.78	21.37
5	2	14.96	-8.76	-5.32	8.75
5	3	0.82	-10.98	1.45	-4.38
5	4	5.68	5.88	-10.63	13.23
5	5	20.67	16.59	4.27	1.99
6	0	-8.06		4.75	
6	1	-7.95	-8.26	-6.55	-1.69
6	2	2.80	-9.08	2.30	3.85
6	3	-1.48	-15.62	-1.28	-2.60
6	4	17.77	1.71	5.55	9.04
6	5	-2.87	11.49	-2.84	10.43
6	6	-5.71	0.82	-11.36	-4.53

Coefficients of the NSWC tide P_1.

n	m	a_{nm}	b_{nm}	c_{nm}	d_{nm}
0	0	1.64		1.82	
1	0	3.28		-10.85	
1	1	4.12	-1.50	0.49	-2.80
2	0	-3.71		-2.81	
2	1	-5.10	-14.59	4.81	-15.14
2	2	8.38	0.99	-1.02	9.58
3	0	3.84		5.19	
3	1	-2.49	1.27	10.41	10.28
3	2	1.48	7.03	1.90	15.37
3	3	-13.79	-14.86	-2.39	-13.26
4	0	1.53		5.28	
4	1	-17.72	6.78	2.38	-9.58
4	2	4.29	3.54	-5.72	2.89
4	3	-4.80	0.76	5.59	-9.48
4	4	3.20	15.59	4.85	5.68
5	0	-6.67		-3.08	
5	1	10.70	-1.70	-6.61	6.61
5	2	4.45	-2.44	-1.63	2.76
5	3	0.28	-2.86	0.87	-1.48
5	4	1.56	2.54	-3.39	4.39
5	5	6.43	5.15	0.69	0.76
6	0	-2.53		1.63	
6	1	-2.52	-2.54	-1.92	-0.16
6	2	1.73	-2.17	0.36	2.12
6	3	-0.22	-5.31	-0.63	-0.80
6	4	5.62	0.02	1.19	2.63
6	5	-0.60	3.63	-0.86	2.90
6	6	-1.84	0.68	-2.83	-1.42

Coefficients of the NSWC tide O_1.

n	m	a_{nm}	b_{nm}	c_{nm}	d_{nm}
0	0	0.27		-2.96	
1	0	4.46		-20.98	
1	1	5.99	-6.29	0.52	-7.16
2	0	9.92		-7.55	
2	1	-18.09	-40.39	11.80	-35.04
2	2	16.92	5.96	-7.87	18.49
3	0	3.44		8.80	
3	1	15.31	15.42	20.71	32.63
3	2	7.97	24.55	-7.50	18.49
3	3	-32.88	-39.43	3.47	-12.47
4	0	-3.41		20.77	
4	1	-36.79	6.42	13.78	-23.33
4	2	9.05	12.42	-12.96	7.23
4	3	-2.56	-4.65	15.71	-27.38
4	4	5.36	27.73	0.07	2.61
5	0	-12.10		-1.23	
5	1	25.65	0.17	-14.53	16.37
5	2	9.13	-2.69	-4.52	3.93
5	3	1.72	-8.12	-0.44	-0.60
5	4	5.47	9.78	-2.07	4.50
5	5	14.98	6.98	-1.35	3.36
6	0	-7.95		4.67	
6	1	-7.39	-3.61	-1.18	-3.08
6	2	6.10	0.16	0.21	5.33
6	3	0.60	-9.00	0.67	-1.23
6	4	11.45	7.04	-4.59	3.82
6	5	1.19	8.03	2.43	5.07
6	6	-6.02	-1.91	-0.35	-4.20

Coefficients of the NSWC tide Q_1.

n	m	a_{nm}	b_{nm}	c_{nm}	d_{nm}
0	0	2.10		-0.29	
1	0	0.60		-4.61	
1	1	0.13	-2.16	0.07	-0.24
2	0	1.57		-2.33	
2	1	-5.04	-9.49	2.08	-6.79
2	2	2.80	0.80	-2.06	2.90
3	0	1.14		1.34	
3	1	4.92	5.59	2.10	6.01
3	2	2.18	4.73	-1.90	2.46
3	3	-7.50	-6.94	2.41	0.23
4	0	-0.47		5.00	
4	1	-6.66	-0.04	4.13	-5.05
4	2	1.67	3.53	-3.59	1.29
4	3	-0.21	-2.51	2.70	-6.58
4	4	0.81	4.93	-0.03	0.10
5	0	-2.13		0.26	
5	1	5.58	0.25	-3.76	3.99
5	2	2.17	-0.45	-1.24	0.48
5	3	0.27	-1.73	-0.23	-0.04
5	4	1.44	1.61	-0.77	0.30
5	5	2.88	1.16	-0.43	0.18
6	0	-1.51		1.23	
6	1	-1.14	-0.89	-0.17	-1.03
6	2	1.23	-0.03	-0.37	0.54
6	3	-0.04	-1.71	-0.14	-0.40
6	4	2.11	1.53	-1.73	0.05
6	5	0.78	1.42	0.79	0.61
6	6	-0.71	-0.37	-0.16	-1.09

Coefficients of the NSWC tide M_f.

n	m	a_{nm}	b_{nm}	c_{nm}	d_{nm}
0	0	1.93		0.23	
1	0	0.98		2.54	
1	1	0.20	-0.52	-0.51	0.18
2	0	-20.49		-6.61	
2	1	-0.69	-0.32	-0.12	1.03
2	2	-0.25	-0.33	0.96	0.09
3	0	1.23		-1.59	
3	1	0.59	-2.26	0.78	-0.20
3	2	-2.08	-0.14	-0.07	-0.22
3	3	0.29	1.57	0.33	1.29
4	0	5.38		-1.23	
4	1	0.16	-0.74	0.18	0.60
4	2	-1.70	-0.68	1.09	0.66
4	3	-0.72	-1.13	-0.15	0.72
4	4	1.16	3.11	0.17	0.56
5	0	-3.25		-3.58	
5	1	-1.07	-1.15	0.21	-0.28
5	2	-1.23	-1.63	-0.15	-0.51
5	3	0.94	-2.21	-0.38	0.93
5	4	-0.54	-0.64	-0.93	0.54
5	5	0.09	1.41	-0.08	-0.08
6	0	1.35		-0.43	
6	1	-0.55	1.22	-0.28	-0.13
6	2	-1.60	-1.04	-0.95	0.22
6	3	1.05	-1.69	0.55	0.79
6	4	0.39	-1.11	-0.45	-0.22
6	5	-0.03	-0.22	-0.70	-0.14
6	6	-0.13	0.45	0.13	0.08

Coefficients of the NSWC tide M_m.

n	m	a_{nm}	b_{nm}	c_{nm}	d_{nm}
0	0	2.50		3.93	
1	0	2.07		-0.80	
1	1	2.32	-0.06	1.05	-0.04
2	0	-13.16		-2.61	
2	1	-0.01	2.03	2.30	2.20
2	2	0.14	1.17	-0.64	0.29
3	0	0.81		-0.10	
3	1	0.91	-0.79	-0.07	-0.88
3	2	-1.02	0.83	1.41	0.55
3	3	1.07	3.01	-0.33	2.35
4	0	1.69		0.62	
4	1	0.32	-0.71	-0.12	0.08
4	2	0.03	0.19	-1.62	0.94
4	3	-0.72	0.26	-1.29	0.31
4	4	0.67	1.97	-0.05	1.20
5	0	-3.45		1.43	
5	1	-1.24	-0.87	0.47	0.14
5	2	-0.40	-0.63	0.31	-0.09
5	3	0.52	-0.14	1.52	1.04
5	4	-0.81	-0.34	-0.62	0.94
5	5	-0.75	0.79	0.16	0.75
6	0	0.66		0.75	
6	1	-1.51	1.07	-1.54	-0.50
6	2	-0.90	-0.27	-0.38	0.39
6	3	0.36	0.20	-0.02	0.41
6	4	-0.63	-0.12	-0.74	-0.68
6	5	-0.62	-0.60	-0.56	-0.86
6	6	-0.36	0.49	-0.22	-0.17

Coefficients of the NSWC tide S_{sa}.

n	m	a_{nm}	b_{nm}	c_{nm}	d_{nm}
0	0	-10.50		16.35	
1	0	6.08		-8.74	
1	1	4.42	0.99	5.49	-5.27
2	0	-10.48		-11.61	
2	1	-2.04	-1.39	2.78	6.74
2	2	6.15	4.52	-2.12	3.50
3	0	0.19		0.73	
3	1	1.90	-1.85	3.89	-0.47
3	2	-7.14	0.24	-1.44	2.84
3	3	0.35	-0.95	-2.17	4.72
4	0	2.94		-0.03	
4	1	-0.21	-0.24	-0.20	-0.60
4	2	-0.85	-0.86	0.78	3.82
4	3	-0.64	-1.26	-2.13	-1.30
4	4	0.29	-0.47	2.35	3.00
5	0	-4.09		-1.30	
5	1	-3.01	-1.60	-2.33	-0.11
5	2	-0.35	-2.10	0.93	-0.65
5	3	0.23	-0.48	0.29	0.15
5	4	0.40	-1.89	-0.62	-0.80
5	5	-0.44	0.97	0.38	2.01
6	0	3.87		-5.61	
6	1	-1.18	0.32	-1.56	-0.81
6	2	-1.47	-2.43	-0.02	-0.36
6	3	1.67	-0.15	1.62	1.62
6	4	0.90	0.61	-0.20	0.21
6	5	-0.18	1.64	-0.47	0.28
6	6	-0.01	1.00	-0.32	0.71

Appendix C Atlas of Load Tide Maps

On the following pages is an atlas of co-amplitude and co-phase maps for 10 of the load tides corresponding to particular constituents of the NSWC ocean tide model. These constituents are (in order of increasing period) K_2, S_2, M_2, N_2, K_1, P_1, O_1, Q_1, M_f, M_m. As noted above, the S_{sa} constituent is not included in this atlas, since a substantial fraction of this tide is non-gravitational and non-loading. The maps were produced using the Gutenberg-Bullen Love numbers as tabulated by *Farrell* (1972). All maps are on the Miller cylindrical projection.

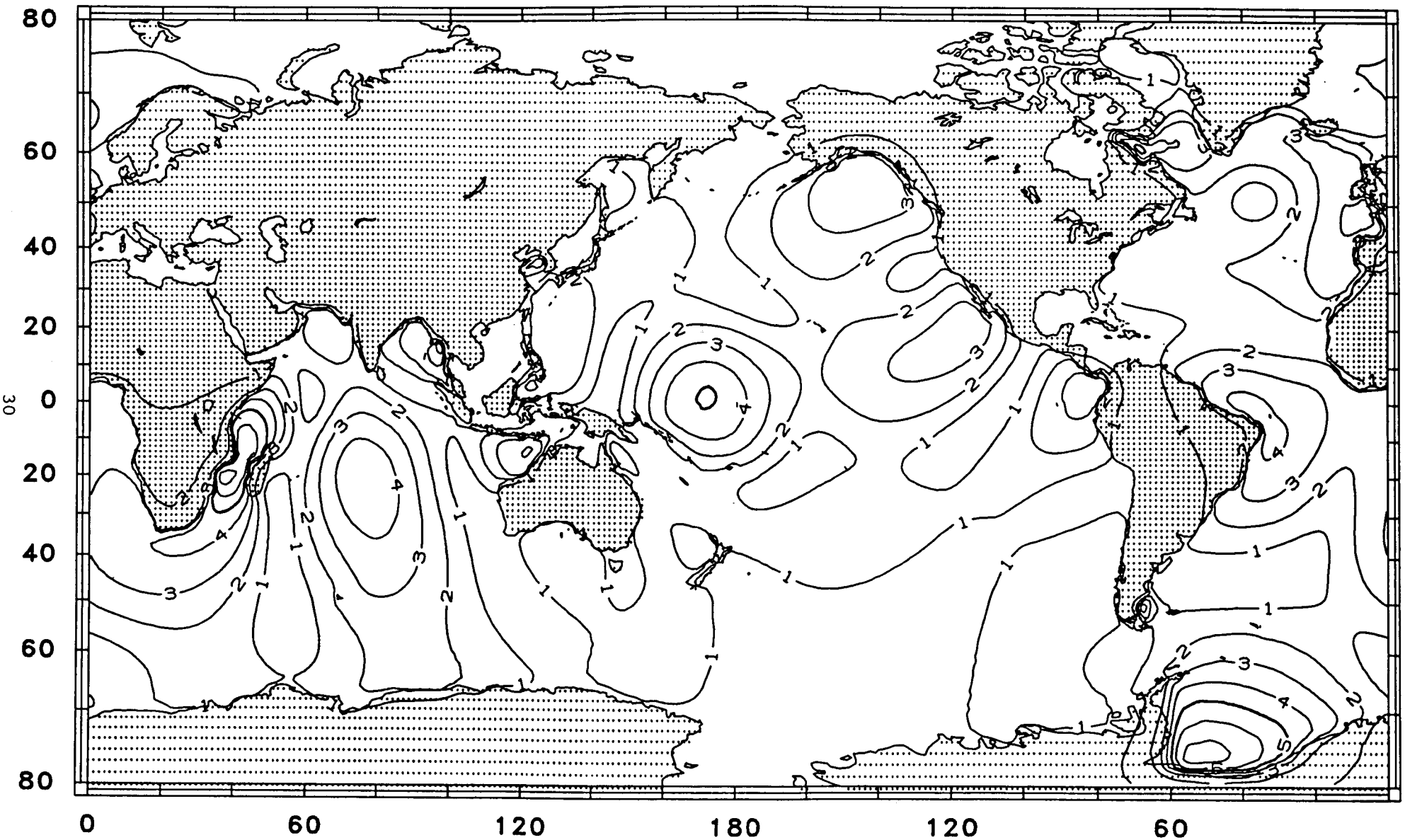

Figure C1. Co-amplitude map for the K_2 load tide (mm).

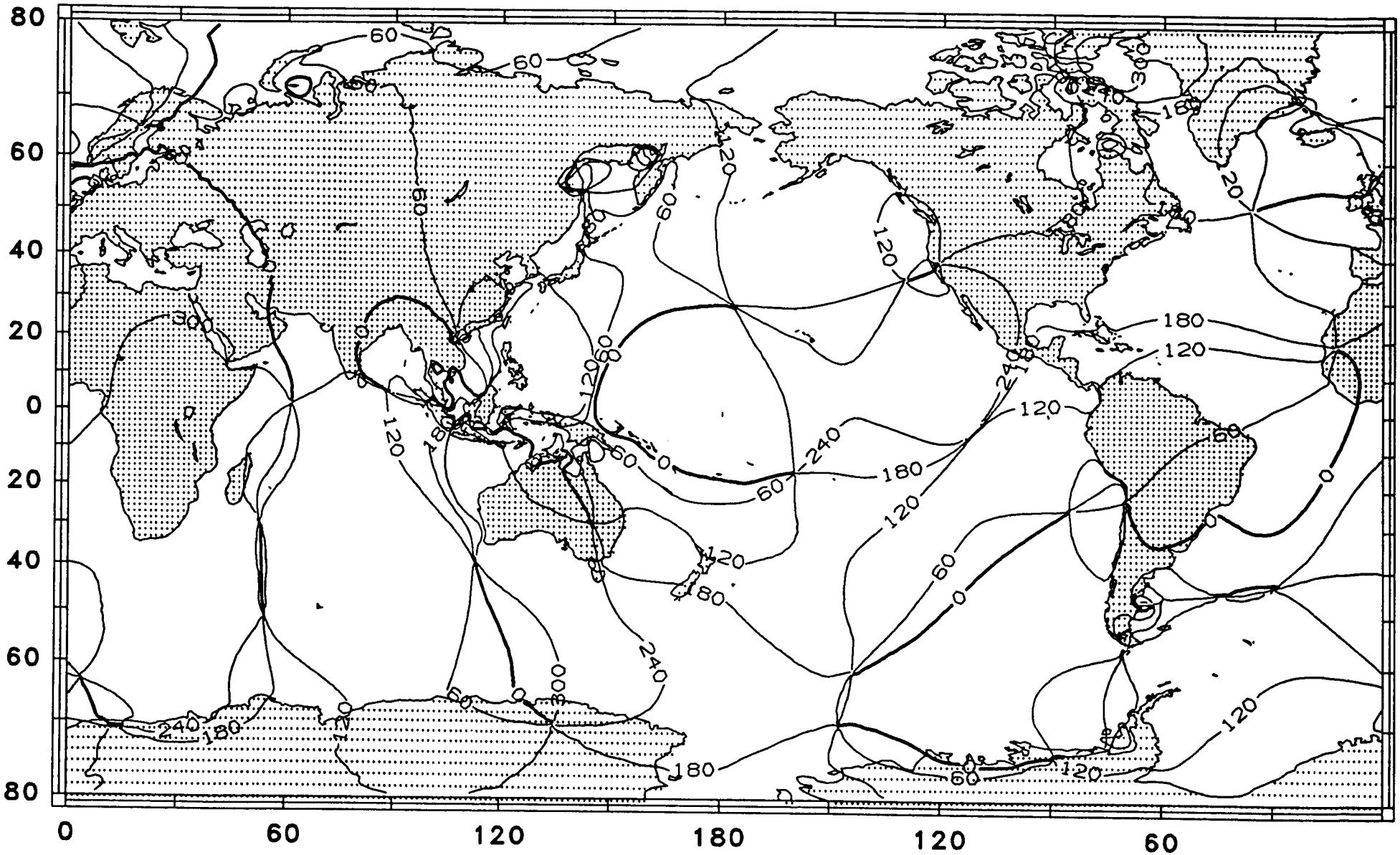

Figure C2. Co-phase map for the K_2 load tide.

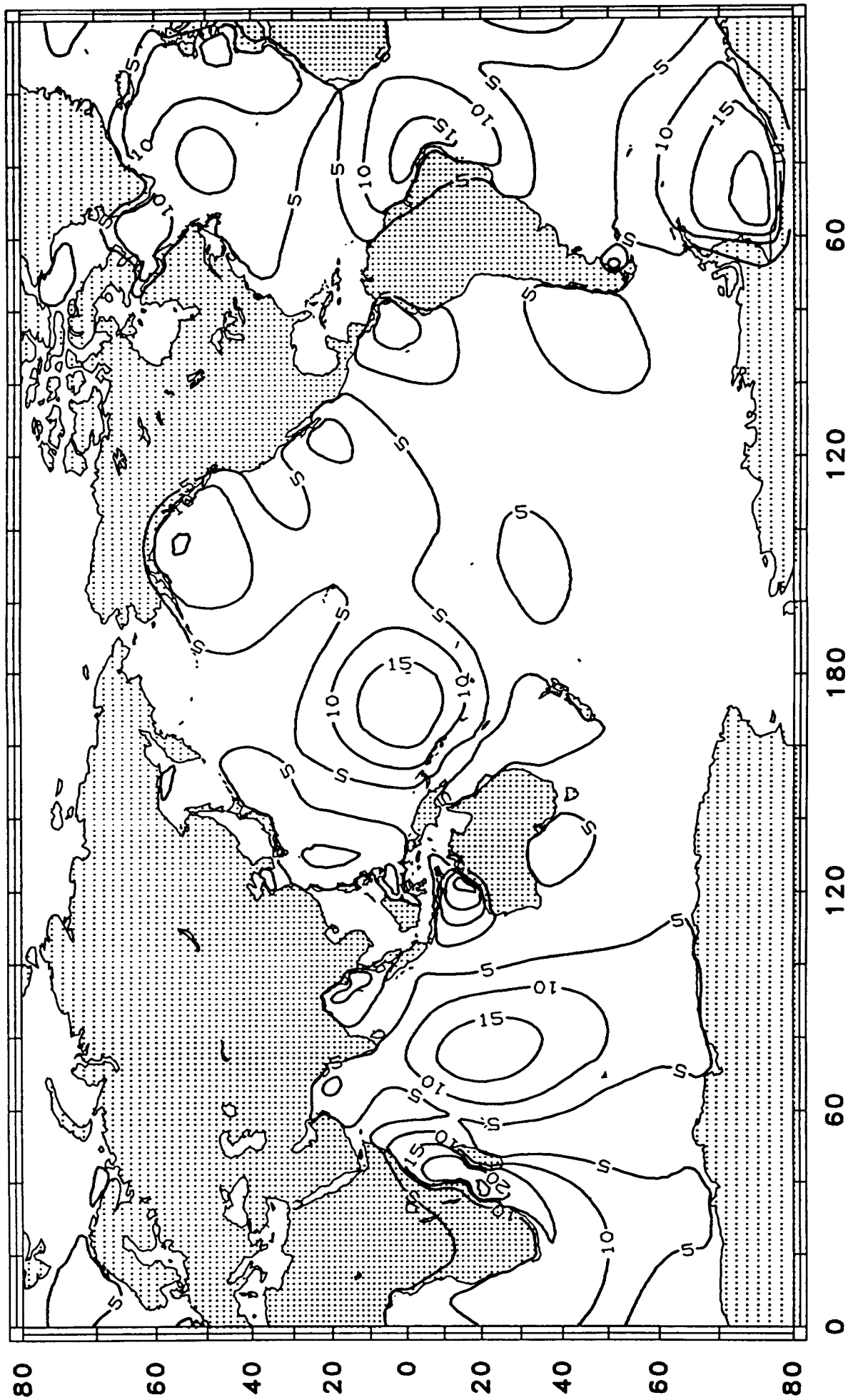

Figure C3. Co-amplitude map for the S_2 load tide (mm).

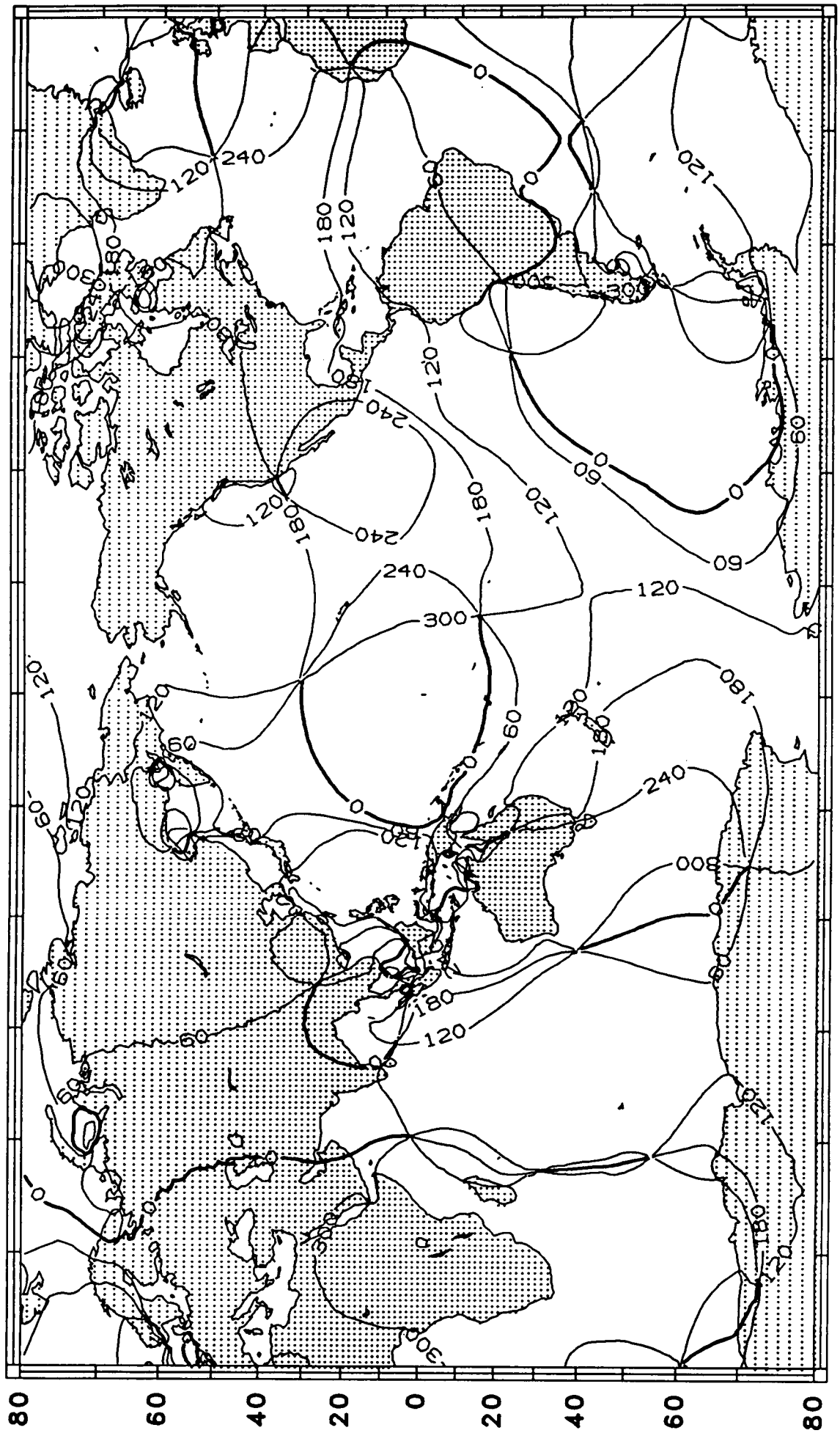

Figure C4. Co-phase map for the S_2 load tide.

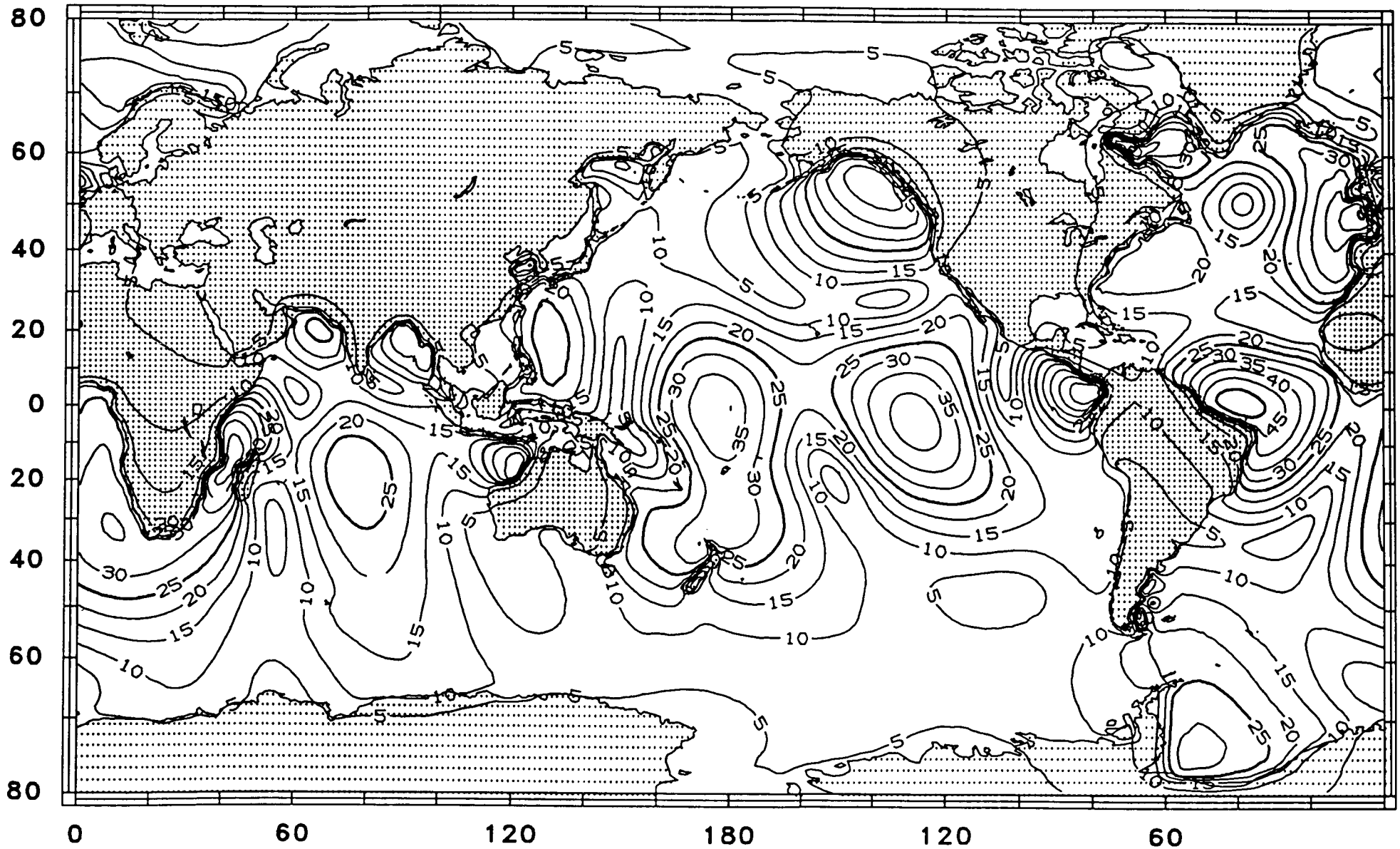

Figure C5. Co-amplitude map for the M_2 load tide (mm).

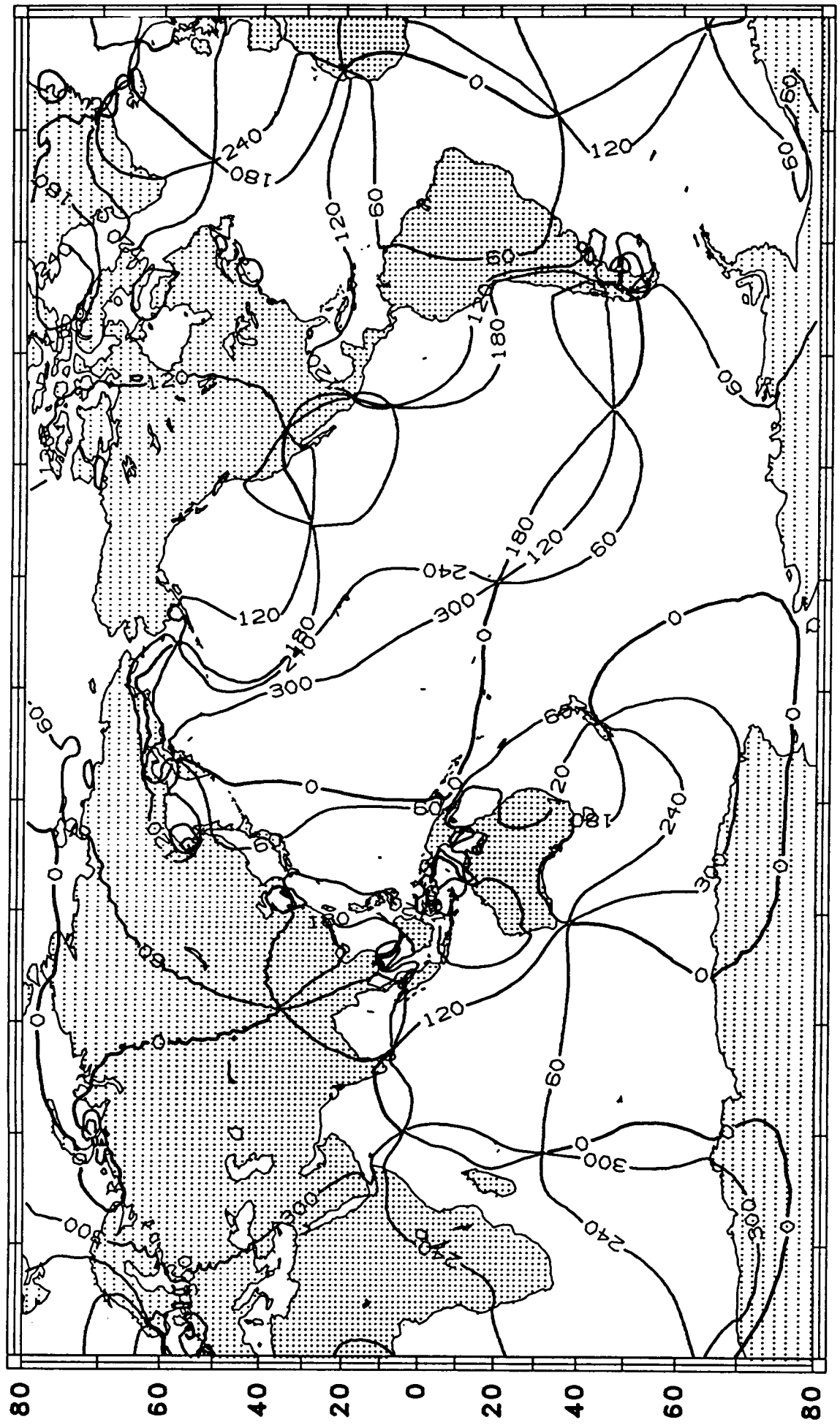

Figure C6. Co-phase map for the M_2 load tide.

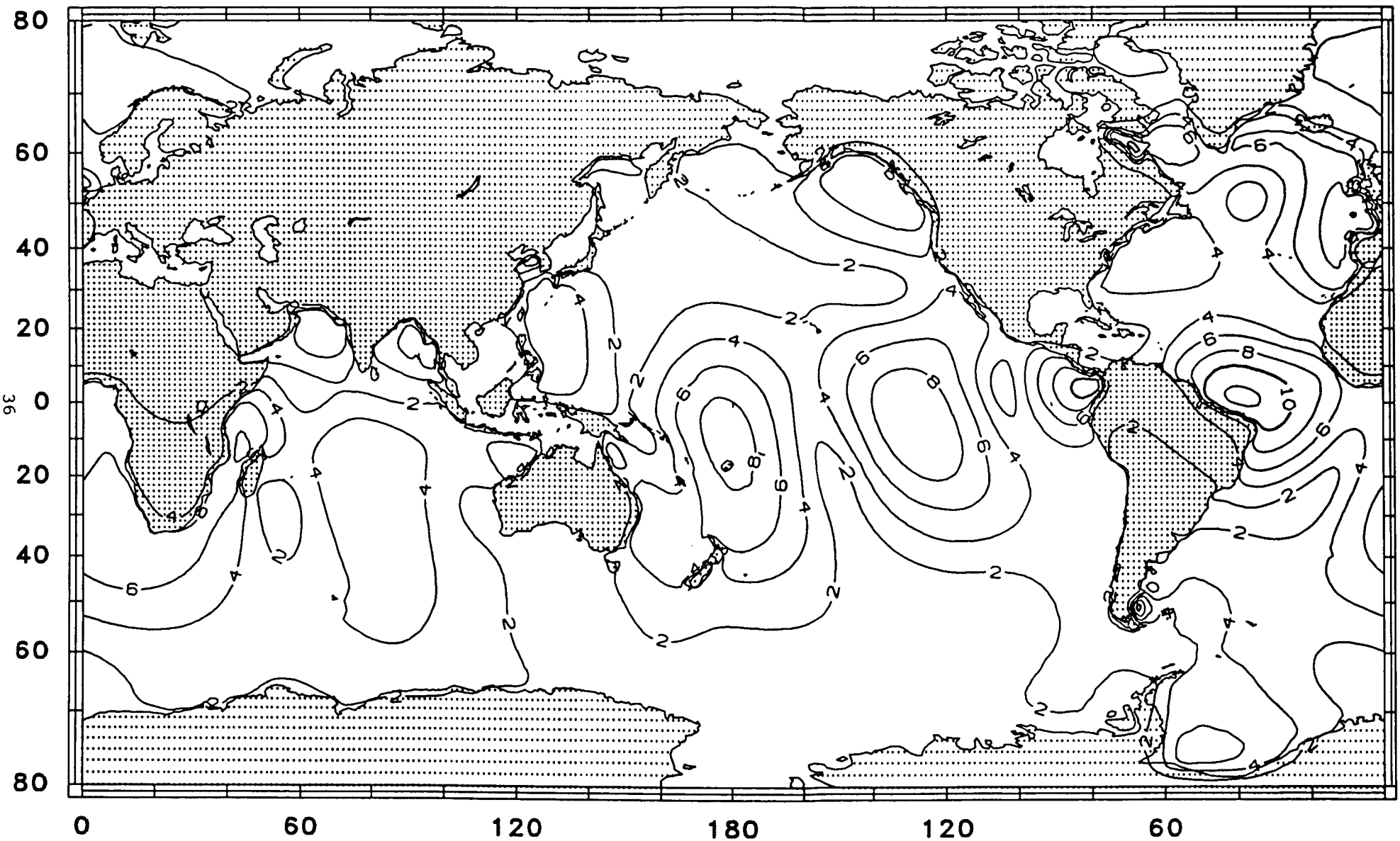

Figure C7. Co-amplitude map for the N_2 load tide (mm).

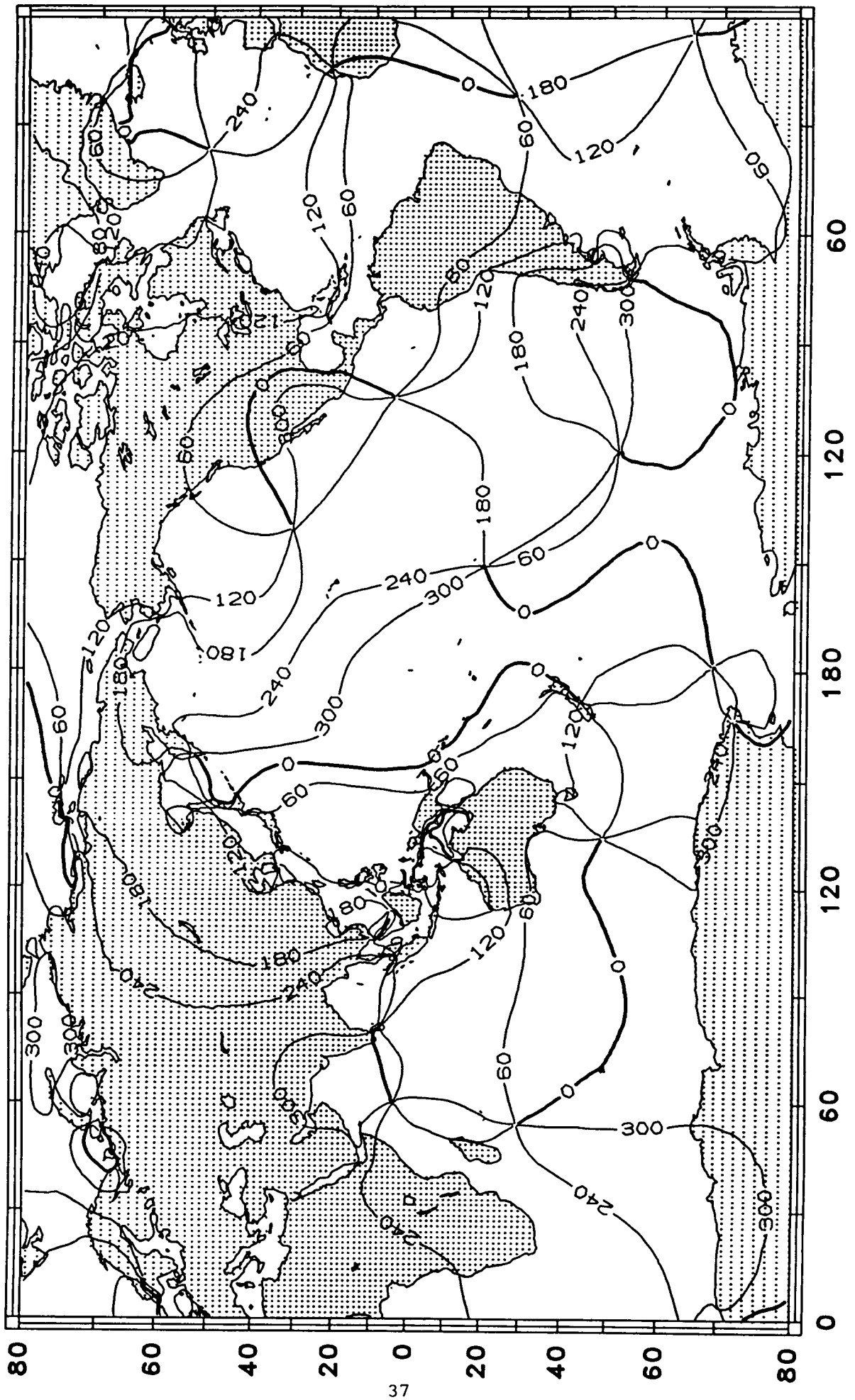

Figure C8. Co-phase map for the N_2 load tide.

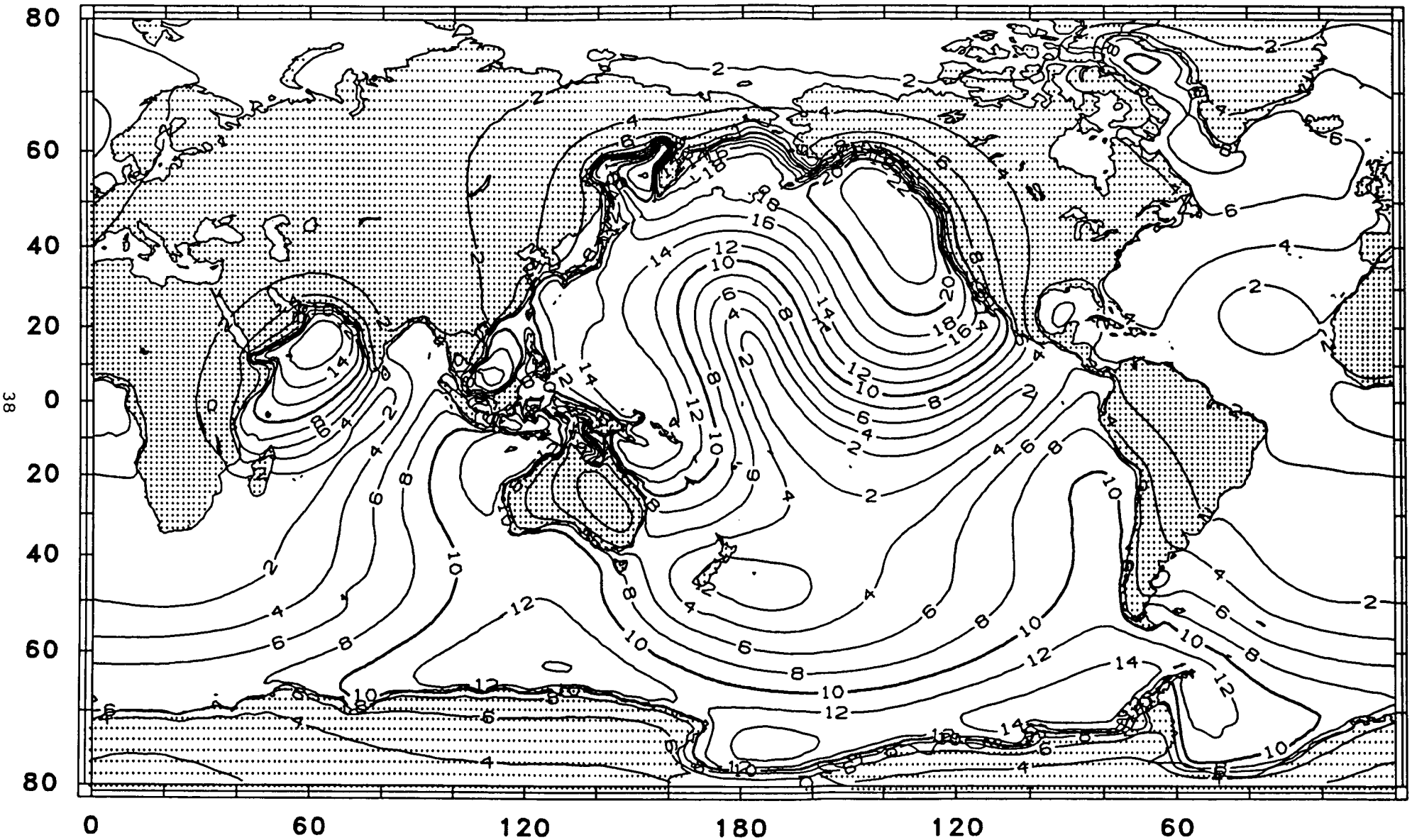

Figure C9. Co-amplitude map for the K_1 load tide (mm).

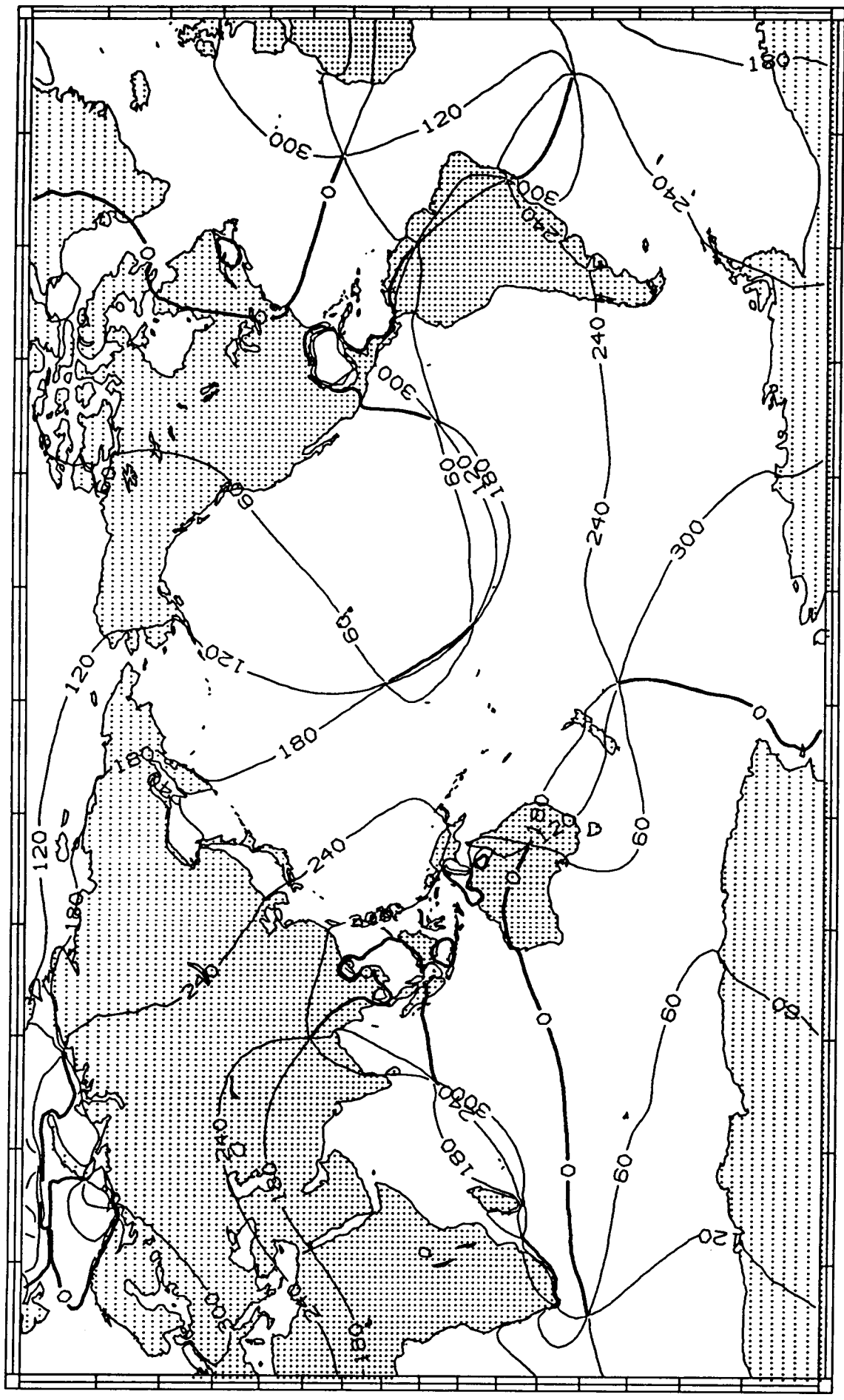

Figure C10. Co-phase map for the K_1 load tide.

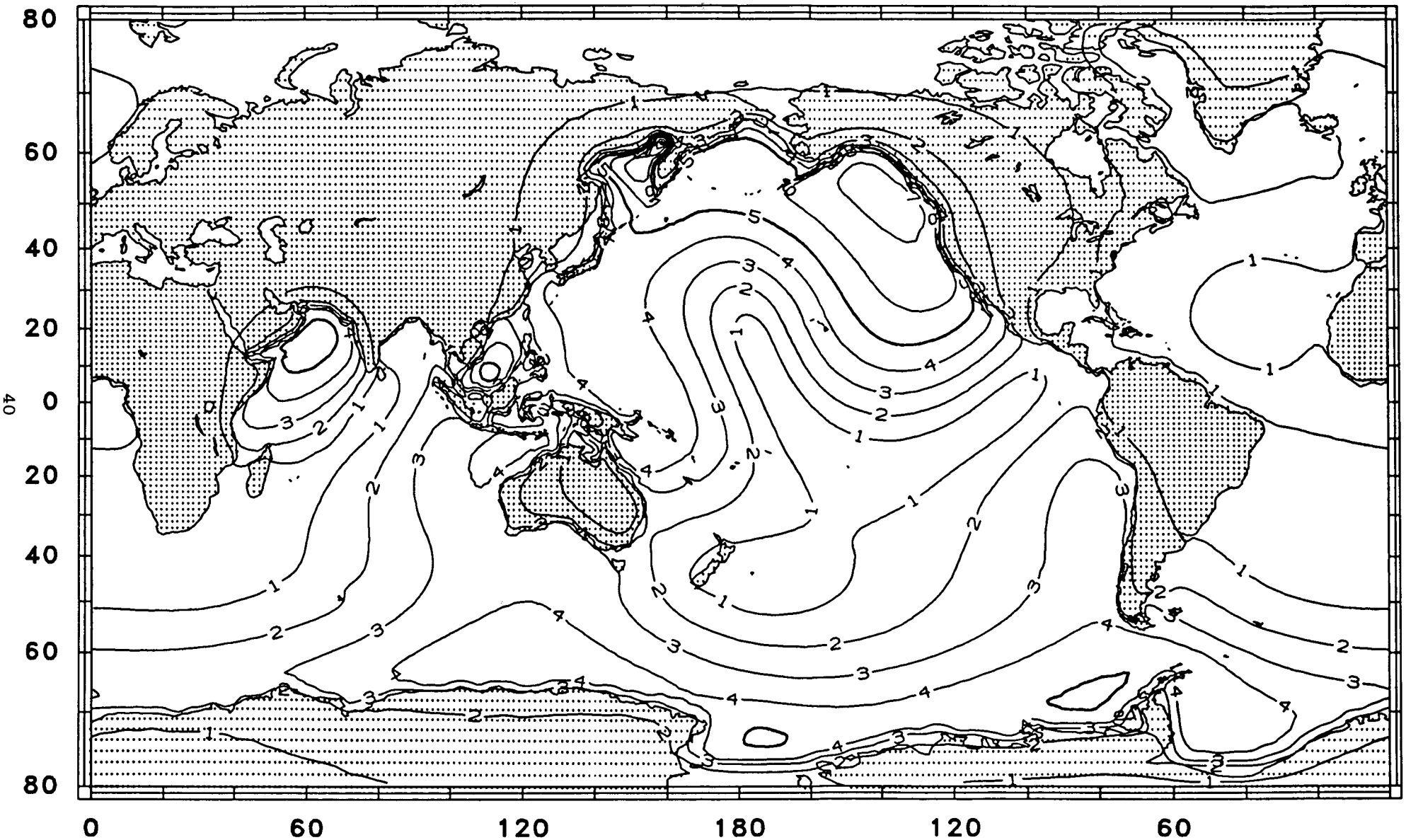

Figure C11. Co-amplitude map for the P_1 load tide (mm).

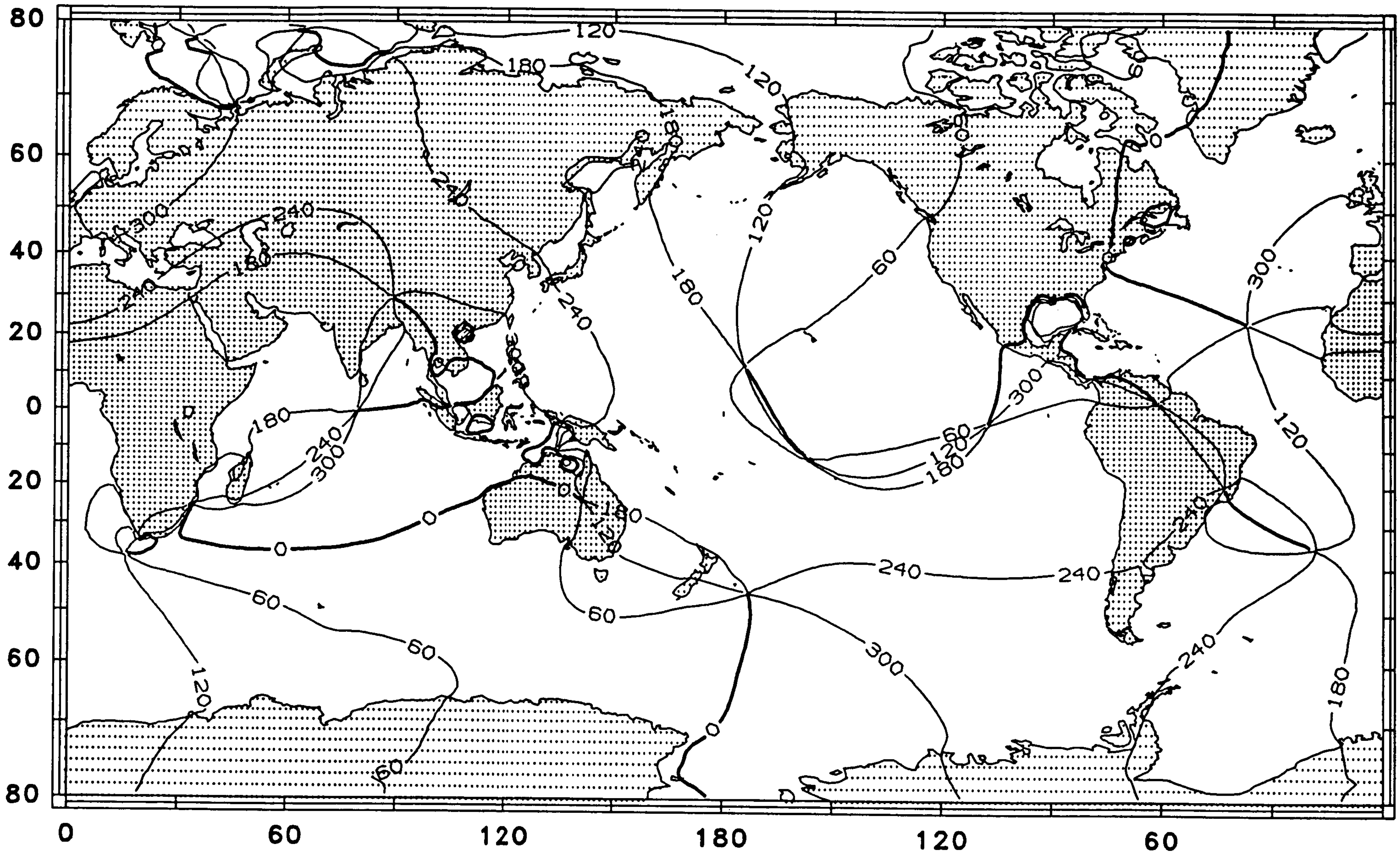

Figure C12. Co-phase map for the P_1 load tide.

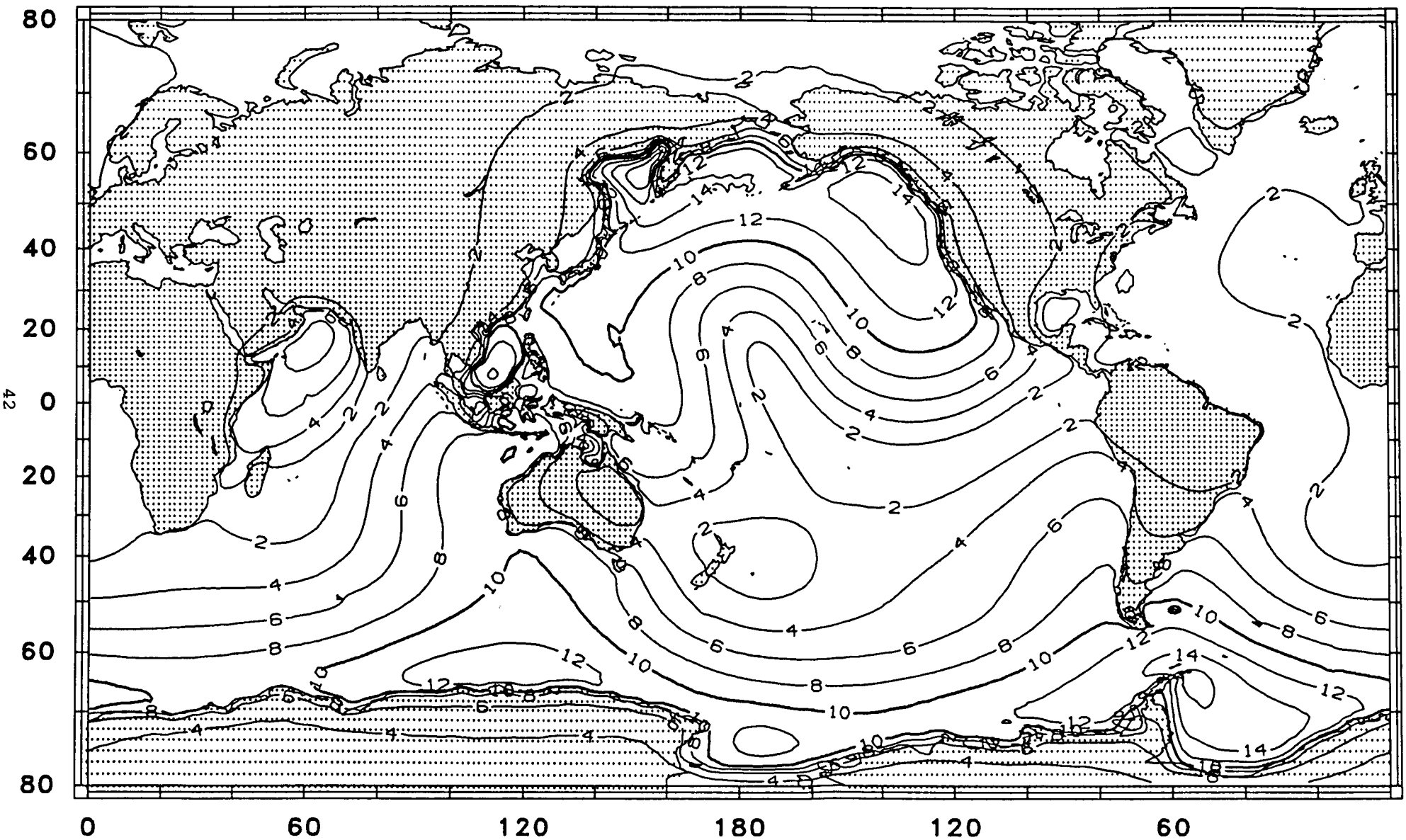

Figure C13. Co-amplitude map for the O_1 load tide (mm).

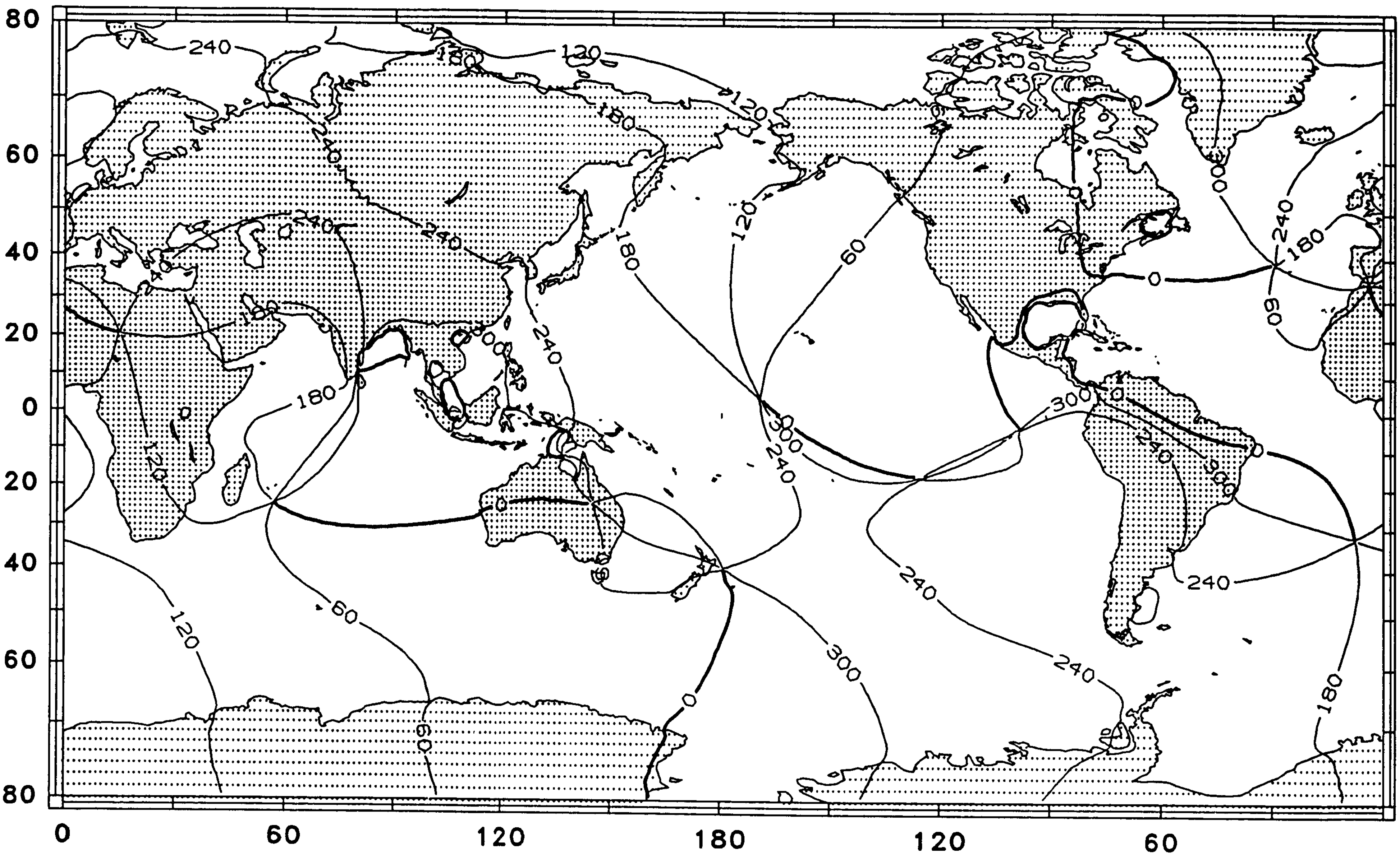

Figure C14. Co-phase map for the O_1 load tide.

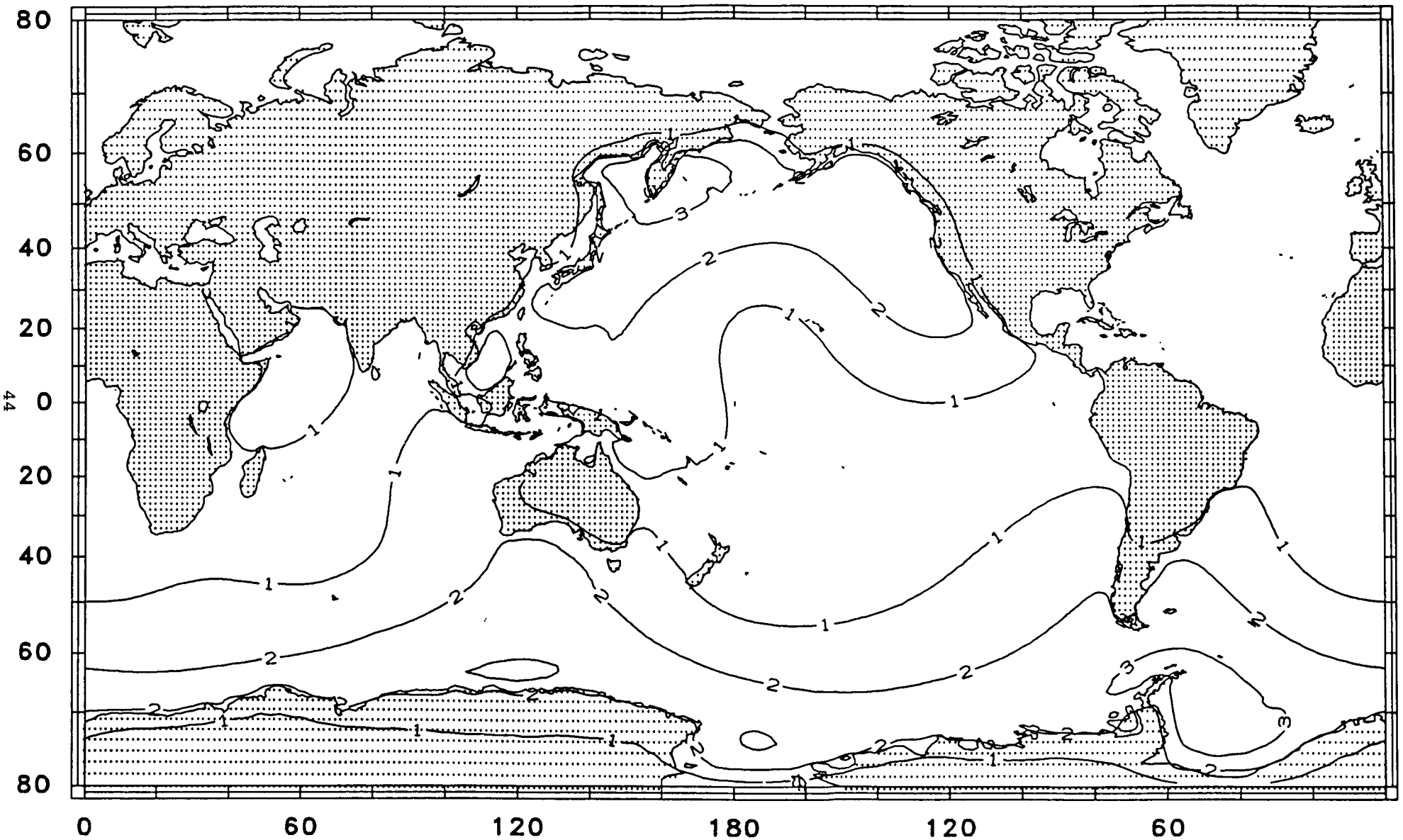

Figure C15. Co-amplitude map for the Q_1 load tide (mm).

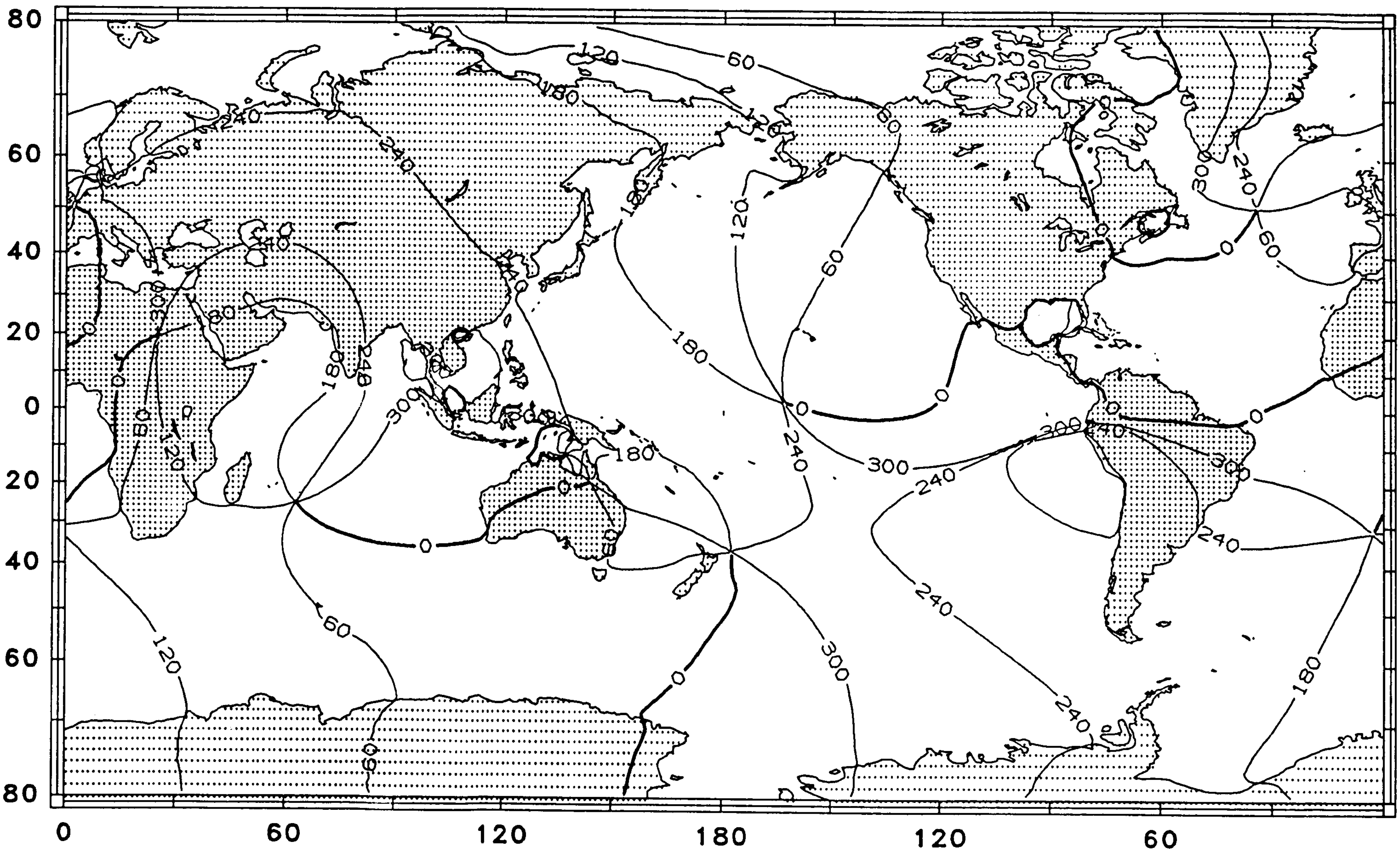

Figure C16. Co-phase map for the Q_1 load tide.

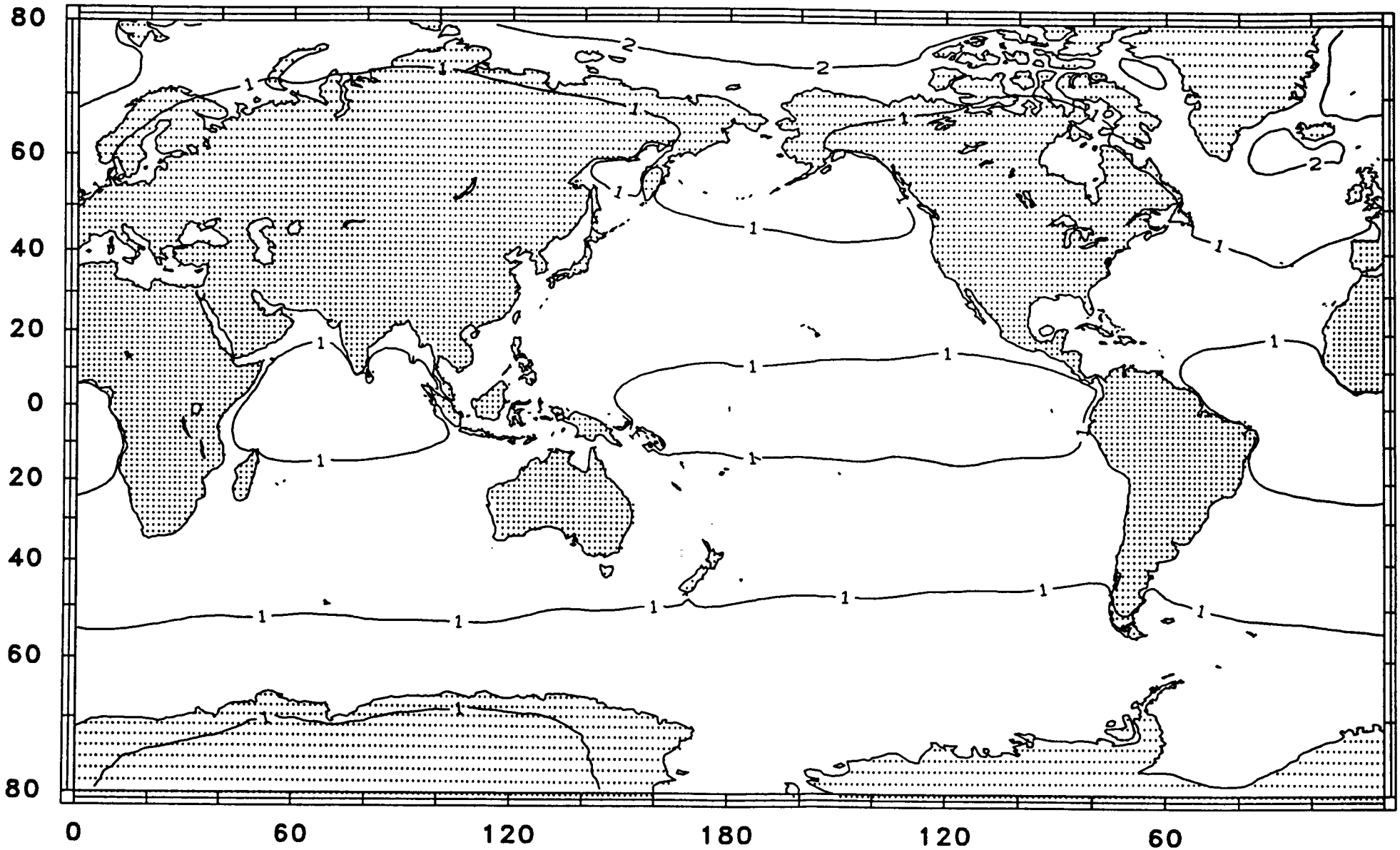

Figure C17. Co-amplitude map for the M_f load tide (mm).

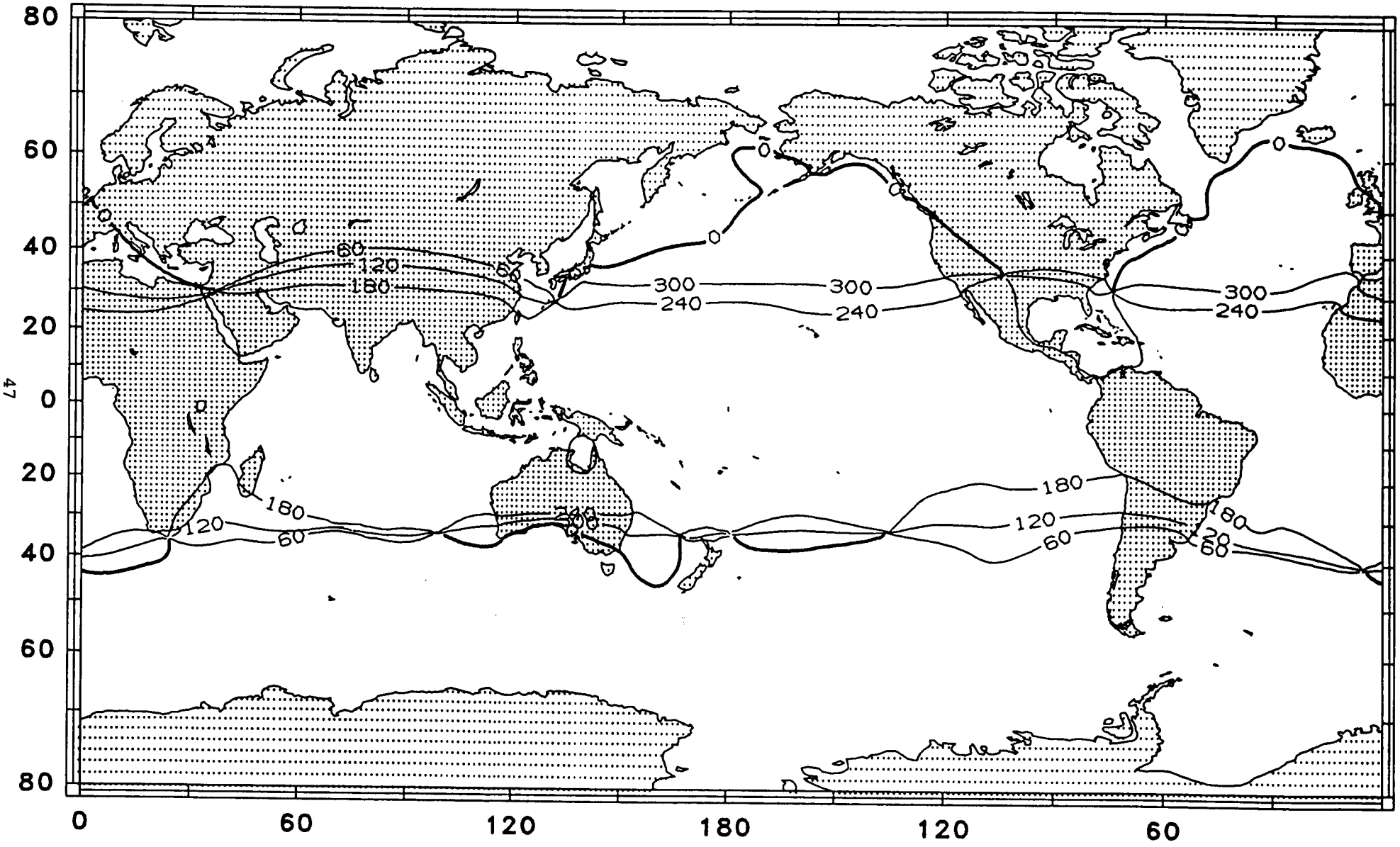

Figure C18. Co-phase map for the M_f load tide.

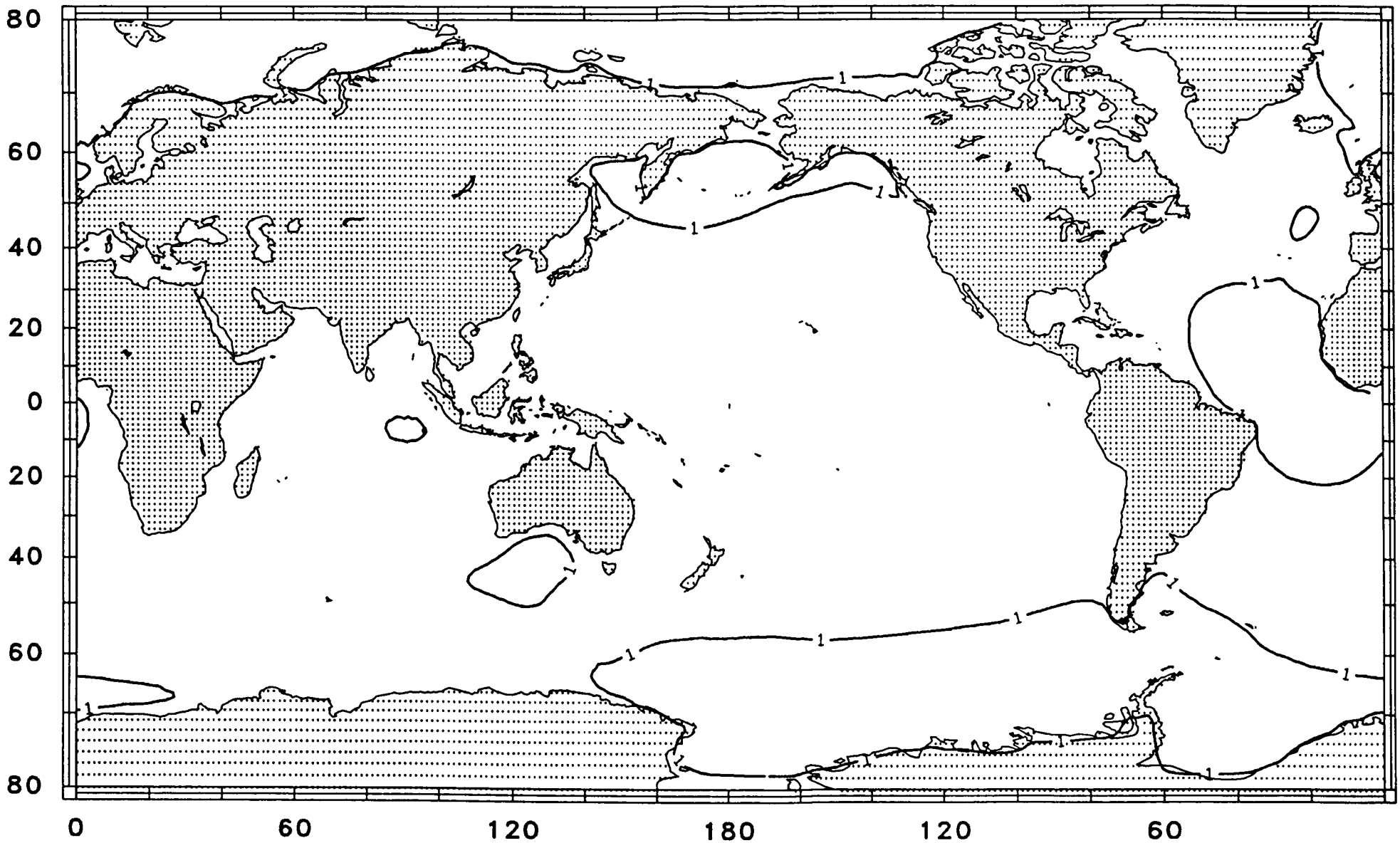

Figure C19. Co-amplitude map for the M_m load tide (mm).

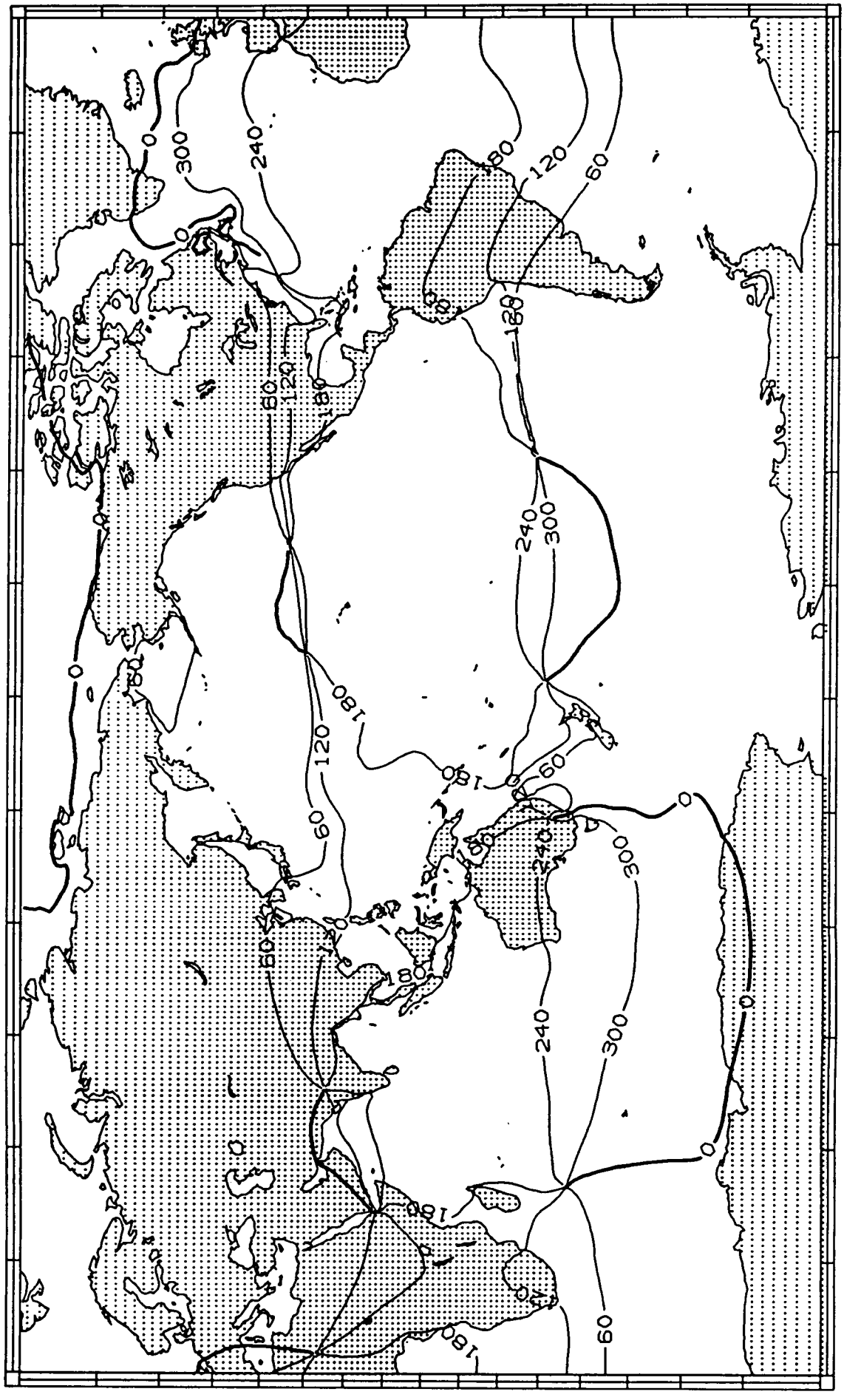

Figure C20. Co-phase map for the M_m load tide.

NASA
National Aeronautics and Space Administration

Report Documentation Page

1. Report No.	2. Government Accession No.	3. Recipient's Catalog No.
NASA TM-100743		

4. Title and Subtitle	5. Report Date
Radial Deformation of the Earth by Oceanic Tidal Loading	July 1989
	6. Performing Organization Code: 626.0
7. Author(s): R.D. Ray and B.V. Sanchez	8. Performing Organization Report No.: 89-154
	10. Work Unit No.
9. Performing Organization Name and Address: Space Geodesy Branch, Goddard Space Flight Center, Greenbelt, Maryland 20771	11. Contract or Grant No.
	13. Type of Report and Period Covered: Technical Memorandum
12. Sponsoring Agency Name and Address: National Aeronautics and Space Administration, Washington, D.C. 20546-0001	14. Sponsoring Agency Code

15. Supplementary Notes

R.D. Ray is affiliated with ST Systems Corporation, Lanham, Maryland.

16. Abstract

A high-degree spherical harmonic series is used to compute the radial deformation of the Earth by oceanic tidal loading. By exploiting "fast" numerical transforms, this approach is found to be much more efficient--but no less accurate--than the traditional Green's function approach. The method is used to derive an atlas of load tide maps for 10 constituents of the NSWC ocean tide model.

17. Key Words (Suggested by Author(s))	18. Distribution Statement
Tides, Tidal loading	Unclassified - Unlimited Subject Category 46

19. Security Classif. (of this report)	20. Security Classif. (of this page)	21. No. of pages	22. Price
Unclassified	Unclassified	51	